Axisymmetric Oscillations of an Opposing Jet
from a Hemispherical Nose

（ 半球頭部からの逆噴射ジェットの軸対称振動 ）

Masahiro Fujita

藤 田 昌 大

①

Axisymmetric Oscillations of an Opposing Jet from a Hemispherical Nose

（半球頭部からの逆噴射ジェットの軸対称振動）

Masahiro Fujita

藤田昌大

It's so beautiful, you see, so beautiful.

—J. D. Watson

Acknowledgments

Abstract

The opposing jet problem has attracted many researchers for a long time because of not only the good applications but also the physical complexity. Especially, the oscillations of flow observed in certain conditions have been unsolved in spite of many previous investigations. This study attempts to give a reasonable interpretation on the mechanism of the oscillations by a method of a numerical experiment. The flow field around a hemispherical nose with a sonic jet issuing from its stagnation embedded in a free stream of Mach 2.5 is computed using the axisymmetric Navier-Stokes equations. Five total pressure ratios of a jet to a free stream, $p_{0j}/p_{0\infty}$ = 0.816, 0.968, 1.005, 1.036 and 1.633 are examined to obtain the flow fields in the stable, unstable and transitional region. In the stable region where the entire flow field is nearly stable except a slight unsteadiness, the computed flow field oscillates about its neutral position in a small amplitude. An oscillating flow model is developed that explains the occurrence of a self-excited oscillation of the free stagnation and the Mach disk. In the unstable region where the bow shock and the jet oscillate drastically, the computed flow field exhibits the remarkable change of the jet structure and its surrounding pressure. An oscillating flow model is developed that explains the feedback mechanism and predicts the amplitude approximately. In the transitional region, the computed flow field changes from one type to another type for the similar total pressure ratio as in the measurement. The condition of transition is confirmed quantitatively in the present numerical experiment.

Contents

Nomenclatures

c	Speed of sound
D	Model diameter
d	Jet exit diameter
e	Energy
f	Non-dimensional frequency
H	Enthalpy
j	Index for grid points in the circumferential direction
k	Index for grid points in the normal direction to the body
l	Distance from the Mach disk to the free stagnation
M	Mach number
p	Pressure
Pr	Prandtl number
R	Gas constant
Re	Reynolds number
r	Spatial coordinate normal to the model axis
s	Distance from the jet exit to the intersecting shock in a free jet
T	Absolute temperature
T_1	Period of the oscillation in the stable region
T_2	Period of the oscillation in the unstable region
T_c	Characteristic time lag
t	Non-dimensional time
U	Contravarient velocity component along the ξ axis
u	Velocity component along the x axis

1

V	Contravarient velocity component along the η axis
v	Velocity component along the r axis
x	Spatial coordinate along the model axis
w	Length of the first cell of a free jet
α	Ratio of displacement of the free stagnation and the Mach disk
γ	Ratio of specific heat
η	Transformed coordinate normal to the body
μ	Dynamic viscosity coefficient
ξ	Transformed coordinate along the body
ρ	Fluid density
τ	Shear stress

Subscript:

b	Values on the bow shock
d	Values on the Mach disk
j	Values on the jet exit
s	Evaluated in the recirculating region
st	Values on the free stagnation
∞	Evaluated in the free stream
0	Stagnation values

Superscript:

n	Evaluated at time $n\Delta t$
$n+1$	Evaluated at time $(n+1)\Delta t$
$'$	Evaluated behind a shock wave

Chapter 1 Introduction

A kind of opposing jets has been introduced originally as one of devices to decelerate space vehicles during a descending trajectory. It is the only effective means of decelerating a vehicle outside the atmosphere. Its effectiveness as a decelerator inside the atmosphere depends on how the opposing jet will affect the pressure drag of a vehicle. Charczenko and Hennessey(1961)[1] have examined the retrorocket effects on the pressure drag of a vehicle that has a spherical nose with a jet exit located in the center. They have found that the retrorocket exhaust causes large reduction of pressure drag in the range of moderate retrorocket thrust at all Mach numbers of the investigation and very large retrorocket thrust will be required to produce decelerating forces much in excess of the jet-off drag forces. Such a large retrorocket is unattractive as a decelerator in the atmosphere because of the large fuel requirements.

From the another view point, opposing jets would be effective devices to reduce the pressure drag of a blunt body. Lopatoff(1951)[2] has investigated the effect of a forward-facing sonic jet on the drag of a blunt body in a transonic flow. He has shown that a separated jet modifies the pressure distribution so as to reduce the pressure drag of the body. Love(1952)[3] has shown that the drag of blunt bodies may be altered by exhausting a small jet from the nose in the case of supersonic free stream.

The another possible application of opposing jets is to alleviate the aerodynamic heating of high speed vehicles. By use of a cold gas jet ejecting from the nose of a vehicle, the aerodynamic heating resulting from

3

considerably high temperature gas behind the strong shock wave is expected to be reduced. Warren(1960)[4] has made an experimental investigation on the heat transfer distribution on a hemispherical nose with helium and air injection. He has found that the stagnation region is cooled locally by mass injection, but that downstream the injected flow reattaches to the nose causing a stagnation annulus that in some case increases the total heat transfer to the nose.

Besides practical objectives described above, the opposing jet flow itself has been of great interest from the physical point of view. A large number of experimental studies concerning the flow field associated with an opposing jet over a blunt nose have appeared since 1950's. Watts(1956)[5] has examined the nature of the flow field caused by the interaction of a sonic jet of fluid directed upstream into a Mach 2.5 free stream. He has managed to classify the regions in the interaction between free stream and jet by optical means. Hayman and McDeamon(1962)[6] have investigated the jet effects on a cylindrical afterbody housing sonic and supersonic nozzles that exhaust against a supersonic stream of Mach 2.9. They have shown that the variation of the ratio of jet total pressure to free stream total pressure, jet exit Mach number and the ratio of jet exit diameter to body diameter have large influences on the body pressure distribution. They have also shown that the free stream Reynolds number has negligible effect on the body pressure distribution. Romeo and Sterret(1963)[7] have investigated the effects of a forward-facing jet of a flat nosed body in a Mach 6 free stream. They have indicated that the flow tends to be very unsteady when the jet total pressure is low and steady flows are found with high jet total pressure, when the jet has a single cell and terminates by a strong normal shock. Finley(1966)[8] has made an experimental study in which an analytical

4

model of the flow is developed and a sufficient condition for steady flow is suggested. He has also indicated the existence of a small oscillation even in nominally steady flow. A detailed examination that contains the measurement of surface pressure distribution has been performed by Karashima and Sato(1975).[9] They have found that the flow field has three kinds of stability regimes such as slightly unstable, very unstable and stable states, depending upon the magnitude of the total pressure ratio of jet to free stream. They have also examined shock detachment distance and location of Mach disk in the stable regime and discussed the dead air pressure in the vicinity of the nozzle exit as well location and strength of the recompression shock wave. Most recently, they have investigated the flow field in the unstable regime by a method of optical observation and measurement of surface pressure distribution.[10] Although a high speed video camera that can take more than 2,000 frames per second has been used in their experiment, they could not find the precise frequency of the oscillation and the detailed flow structure mainly because the oscillations observed such as shock waves were considerably three-dimensional phenomena.

On the other hand, several numerical approaches have been applied on the opposing jet problem since 1970's. Hirose and Kawamura(1971)[11] was the first to investigate numerically the flow field induced by a supersonic opposing jet from a flat-faced nose by a time-dependent finite-difference method. They have obtained two different types of flow field to which they have refereed the steady and unsteady case in the experiments respectively. Satofuka and Matsuno(1975)[12] have computed the flow field over flat-faced- and hemisphere-cylinders with an opposing jet in a supersonic free stream using the Euler equations together with the shock capturing

5

method. In their investigation reasonable agreements between computed and measured data have been shown in the steady flow case. Recently, Macaraeg(1986)[13] has applied the Navier-Stokes equations to a configuration of a counterflow nose jet in a hypersonic free stream using the Beam-Warming algorithm. The computed shock structure shows agreement with experiments, but no pressure measurement is available for comparisons. Fox(1986)[14] has computed the flow field resulting from a sonic opposing jet from a hemispherical nose using the thin-layer Navier-Stokes equations with bow shock fitting method. Good agreements have been achieved for the surface pressure distribution on the body. The author et al.(1991)[15] have computed the flow field of a relatively high total pressure jet and discussed detailed features of the opposing jet flow. Then it has been indicated that the flow is not exactly stable even at the total pressure in which it has been expected to be stable in the most previous experiments.

These previous studies together have covered a wide range of variables and the results may be summarized as follows:

- Most dominant parameter deciding the flow field is the ratio of jet total pressure to free stream total pressure. When the pressure ratio is less than a critical value the flow field becomes unstable and a bow shock remarkably oscillates (*unstable region*). When the pressure ratio is above the value the flow field seems almost stable and a Mach disk can be clearly observed inside the jet (*stable region*).

- The critical value of the total pressure ratio depends on a free stream Mach number and a jet exit Mach number. Around the

6

critical value, the flow field results in either unstable or stable type of flow and it tends to alter from one to another in turn (*transitional region*).

- The ratio of the jet exit diameter to the body diameter affects the critical value in the case of flat-nosed bodies. Decrease in the diameter ratio increases the critical value, in other words, makes the flow field more unstable.

- The nose shape of the blunt body and the Reynolds number of free stream seem to have little influence on the opposing jet flow. The characteristic phenomena of the opposing jet flow described above are observed on both spherical and flat-faced noses of blunt bodies regardless of the Reynolds number.

At the present time we could obtain a large amount of basic knowledge on the opposing jet flow from the results of these successful investigations. These studies, however, have been mainly intended to clarify the flow structure in the stable region and made no detailed analysis in the unstable and transitional region. It is mainly due to the difficulties in the measurement of time-varying flow fields such as bow shock or pressure on the body surface in the wind tunnel experiments. As a temporary standard the current status of research on the opposing jet problem is shown in brief in table 1.

As is evident from the table 1, quantitative results are insufficient in comparison with qualitative ones and we have still little knowledge on the phenomena in the unstable region. Important problems left unsolved are as follows:

- Why does the small oscillation in the stable region occur and how much are the frequency and the amplitude?

- Why does the large oscillation in the unstable region occur and how much are the frequency and the amplitude?

- Why does the transition between the stable and the unstable region occur and what does the threshold depend on?

Table 1   Current status of research on opposing jet problem

	Qualitative results	Quantitative results
Stable region	Good	Fair
Transitional region	Fair	Poor
Unstable region	Poor	Poor

The purpose of the present study is to answer these questions and to develop new models of the flow field that can explain better the various phenomena observed. The author will discuss the opposing jet problem on the basis of results of the free jet studies that have been performed by many researchers for a long time by the method of wind tunnel tests or a variety of computations.[16-26] Although we have never still obtained complete understanding in the field of the free jet, it may be quite well to use many valuable fruits of the free jet studies as right assumptions before the present study. The author will also refer directly the results of previous wind tunnel tests on the opposing jet flow. Although time-varying measurements are not available in the experiment, ordinary schlieren photographs and time-averaged measured surface pressure give at least the macroscopic phases of the phenomena.

8

In the present study the author will employ a method of computation in order to obtain time-varying flow fields. The computational technique has recently achieved great improvements in the field of fluid dynamics. The author here would like to emphasize the point that the present computation intends not to simulate the real flow field but to solve the equations of fluid that are simplified within the limits of preserving essential properties of the problem for obtaining only the most primary phenomenon in the problem. The schematic approach in the present study described above is summarized in Figure 1.1.

In this study the author will deal with the flow field over a hemispherical nose with an opposing jet from its stagnation point. Although very similar phenomena including two different types of flow field are observed on both spherical and flat-nosed bodies as before, the author has the idea that the mechanism of oscillations in both cases should not be identical as described later. Thus the author will here focus attention on the mechanism of oscillations that occurs in the flow field over a hemispherical nose with an opposing jet.

Firstly, in chapter 2 two types of flow field and the transition from one to another will be discussed on basis of results of previous studies. Many important results of wind tunnel tests on flow fields in the stable and the unstable region will be described and a few models of the flow fields suggested by former researchers will be also reviewed by the author to demonstrate the incompleteness of those models. In chapter 3 a series of numerical experiments will be performed to obtain time-varying flow fields. After presenting the numerical method used in detail, a variety of numerical solutions will be discussed associated with validations with

9

experimental data. The author will develop some new models of the flow field in the stable, unstable and transitional regions in chapter 4. Those models can correspond well with the results of wind tunnel tests and numerical experiments here and explain the mechanism of oscillations of the flow field qualitatively. Moreover the author will also illustrate that the new models developed could give quantitatively the frequency or the amplitude of oscillations in the stable and the unstable region.

Chapter 2 Description of flow fields

As is described in chapter 1, it has been found that the flow pattern over a hemispherical nose with an opposing jet tends to change drastically at certain critical value of the total pressure ratio. The flow field have been classified into three different regions such as stable, unstable and transitional region. The terms will also be used in the present study for convenience. In this chapter, the author will discuss the flow field of the opposing jet in detail according to the classification.

2.1 Stable region

Most of studies by experiments referred here has reported that the flow field of the opposing jet is stable at higher total pressure ratios. Figure 2.1 shows an ordinary schlieren photograph of the flow field over a hemisphere-cylinder with a sonic opposing jet at relatively high total pressure ratio ($p_{0_j} / p_{0_\infty} = 1.633$) in a free stream of Mach 2.5.[10] The bow shock and the Mach disk inside the jet are clearly resolved and no evidence of unsteadiness of flow can be observed by this picture. A few of researchers have tried to develop the model of flow field in the stable region by use of photographs like this. Figure 2.2 shows a typical flow model suggested by Finley.[8] The jet separates from the orifice and moves forward to the interface with the mainstream through a terminal shock. The dividing stream line springing from the orifice edge returns to the body surface at the reattachment ring and there is a toroidal recirculation region, dead air region called by Finley, around the jet. The jet layer turns along the model

11

surface at the reattachment ring and flows away downstream. The pressure rise associated with the reattachment of the shear layer causes a turning shock. In summary, the primary effect of the opposing jet is to produce a recirculating region between the separated jet and the body surface, where pressure is much lower than that at the stagnation region on the blunt nose itself.

The flow model of Finley is fairly well constructed, but its coarse structure is inevitable due to the limitations of experimental observations. Fox[14] has developed a slightly more complex model by use of the results of the thin-layer Navier-Stokes computation of flow field. In his model as in Figure 2.3, the jet issuing from the nozzle exit is intercepted by the barrel shock and the Mach disk and the reflected shock occurs from the triple point. Although the Fox's model has not still sufficient fine structure because of a lack of gird points used in his computation, the author thinks that it is possible to construct more correct model of the flow field by use of careful numerical simulations. In the later chapter the author will develop a new finer flow model in the stable region from the results of the numerical experiments.

Several researchers have also tried to predict quantitatively the position of the bow shock, the Mach disk or the interface between jet and mainstream. Preliminary to the detailed analysis, Romeo[7] has applied a one-dimensional inviscid model on the flow along the symmetrical axis and developed the static condition of the flow as

$$p'_{0j} = p'_{0\infty} \tag{2.1}$$

where p_{0j}' is the total pressure of the jet flow after the Mach disk and $p_{0\infty}'$ is the total pressure of the mainstream after the bow shock. Although $p_{0\infty}'$ is constant in a free stream with a specified Mach number, p_{0j}' is the function of the position of the Mach disk since the Mach number just ahead of the Mach disk depends on the distance from the jet exit. Figure 2.4 shows the equilibrium flow model of Romeo. We can obtain the position of the Mach disk by solving the Eq. (2.1) if the explicit form of the function p_{0j}' with respect to the position on the axis is given. The total pressure distribution along the axis of the free jet can be obtained from the solution of sonic jet by the method of characteristic of Owen and Thornhill(1952).[27] Their result agrees well with the result of the measurement of Pitot pressure. Adamson and Nicholls(1959)[28] have also calculated the pressure distribution approximately in free jets for other jet exit Mach numbers. Finley has tried to predict the position of the Mach disk inside an opposing jet by use of the static condition of Romeo and the solutions of Owen et al. then obtained the satisfactory results.

For a sonic free jet expanding into a vacuum, the Pitot pressure is given by an empirical formula as well as the characteristic solution. The simple form of that developed by Ashkenas and Sherman(1966)[29] is as

$$\frac{p_{0j}'}{p_{0j}} = 0.64\left(\frac{x}{d}\right)^{-2.07} \tag{2.2}$$

where p_{0j} is the original total pressure of jet, x is the distance along the axis from orifice and d is the diameter of orifice. Romeo(1965)[30] or Cassanova and Wu(1969)[31] have calculated the position of the Mach disk in an opposing jet using this formula as

13

$$\frac{x_d}{d} = 0.806 \left(\frac{p_{0j}}{p'_{0\infty}} \right)^{0.483} \tag{2.3}$$

The fraction in right member is reexpressed as

$$\frac{p_{0j}}{p'_{0\infty}} = \frac{p_{0j}}{p_{0\infty}} \cdot \frac{p_{0\infty}}{p'_{0\infty}} \tag{2.4}$$

where $p_{0\infty}/p'_{0\infty}$ denotes a ratio of total pressure of a free stream through the bow shock that is a function of a free stream Mach number. The position of the Mach disk obtained by Eq. (2.3) agrees quite well with the characteristic solution as well as the experimental data.

Contrary to the case of the Mach disk, no attempts to predict the position of the bow shock and the interface has resulted in success. Finley has also developed the geometrical flow model that contains spherical coned interface, but it cannot determine the position of the attachment of the jet flow to the body because of the limitations of the inviscid theory. As a result, the pressure in the recirculating region has been given as the function of the attachment angle ε so that the interface and bow shock position also depend on the arbitrary variable ε in his model. It seems that the failure of Finley described above indicates the impossibility to construct any analytical inviscid models of entire flow field including the recirculating region. As is generally known, the viscosity of fluid plays considerably significant roles in recirculating regions and characteristic events such as separation or reattachment of flow usually depends strongly upon viscous effects of fluid including turbulence effects. If the oscillations of the opposing jet flow are controlled essentially by viscosity of fluid, it is considered that any theoretical treatments without the turbulence may not be practical on the oscillation problem. Indeed, is the viscosity of fluid

14

indispensable for the oscillation? The answer given in the present study is *No*. The reason associated with the mechanism of the oscillations will be presented in chapter 4.

2.2 Unstable region

Nearly all studies made so far have mainly focused attention on the flow field in the stable region, so that we have obtained only a very small number of knowledge on the flow field in the unstable region. As is described in last chapter, the greatest reason of that is naturally in the difficulties of measurements of time-varying properties in wind tunnel experiments. Figure 2.5 shows an schlieren photograph of the flow field in the unstable region ($p_{0j} / p_{0\infty} = 0.816$).[10] Both bow shock and Mach disk are dimmed in this picture and a considerable oscillation appears to exist. The frequency of the oscillation of bow shock is assumed to be empirically the order of the hundred or ten times as much per second in the experiment. It is very difficult to measure directly the time variation of the position of the shock wave by the present optical methods because the oscillation is considerably three-dimensional phenomenon as well as is rapid one. Also the measurement of the time variation of surface pressure distribution have been carried out and some meaningful data of the frequency up to 5000 Hz have been obtained, but the correctness of the frequency seems to be slightly doubtful considering the performance of the pressure transducers used. Consequently, we have still never obtained any correct data on the frequency or amplitude of the large oscillation in the unstable region from wind tunnel measurements.

15

From the viewpoint of the mechanism of the oscillation, an oscillatory flow model in the unstable region has been suggested by Fox. The mechanism of the oscillation in his model is as follows: At a low total pressure of an opposing jet, the low speed side of the shear layer of the shorter jet reattaches the nose at a relatively steep angle and is turned back into the recirculating toroidal eddy adjacent to the jet. As the torus grows in time, the attachment angle becomes more shallow with respect to the body surface until part of the eddy is entrained downstream and the eddy shrinks.

The Fox's flow model seems to contain a part of truth. However it can explain only the fluctuation in the recirculating region, but cannot explain how the bow shock moves intensely forward and backward in turn. Besides, if the oscillation is caused by a short jet of the low total pressure, the flow over a hemispherical nose with a physical spike of the same length placed on the stagnation point must oscillate by similar reasoning. The previous investigations including ones by the author et al.[15, 32-34] on the spiked flow has apparently denies the assumption. The flow field over a spiked hemisphere is always stable regardless of the length of the spike.

In the case of the flow field over a spiked flat nose, the flow tends to oscillate in the range of short spike length. Maull[33] has explained the mechanism of the oscillation and the summary is as follows: The separated boundary layer from the short spike strikes the flat face of the body and a detached shock wave is required outside the shear layer. The high pressure behind the shock causes air flow into the recirculating region and enlarges the recirculating region until its shape changes to a blunt-nose configuration forming a nearly normal shock at the spike tip. As the

16

enlarged recirculating region moves the reattachment point towards the shoulder, the reattachment angle decreases and the pressure behind the reattachment shock also decreases. Thus the feeding of air into the recirculating region stops. After moving the reattachment point out of the flat-face, air is now fed from the region out past the shoulder and the recirculating region collapses. When the excess air in the recirculating region has escaped and the separation has occurred at the spike tip again, the cycle begins again. Maull has also presented the critical condition of the oscillation in which the oscillation stops when the spike is lengthened until the reattachment point reaches just the shoulder of the body because of no reattachment shock.

The mechanism of the oscillation in the flow field of a spiked flat-nose described above seems to be reasonable. Let us reconsider the opposing jet problem, the same idea might be applied on the oscillation of the flow field over a flat-nosed body. In the case of the opposing jet, the jet flow turned back at the free stagnation will play the same role as the separated shear layer from the spike and both opened and closed recirculating region will appear in turn. Recently Nishida et al.(1992)[35] have investigated the flow field over a flat nose with an opposing jet by a numerical simulation and have obtained oscillatory solutions at a low total pressure of the jet.

In the case of the spherical nose, the situation seems to be quite different from the flat-nose. The reversed jet flow attaches the body surface at the angle without a detached shock and the recirculating region is always closed. Thus we must construct a new flow model that can explain the oscillation of the opposing jet from a hemispherical nose as well as the steadiness of the flow over a spiked hemispherical nose.

17

2.3 Transitional region

The previous experimental data has stated that the transition between the stable and the unstable region occurs in certain range of the total pressure ratio of a jet to a free stream. It is anticipated that the critical value dividing two types of flow can be theoretically predicted inside some range of total pressure ratio where the transition is observed. Finley has developed a sufficient condition for steady flow in which the condition of transition is described in detail. The condition suggested by Finley is as follows: A supersonic jet contains several jet cells until the flow decelerates to a subsonic flow. If the position of the terminal shock decided by the equilibrium condition in the stable region is in the first jet cell, the approaching flow is independent of the pressure surrounding the jet and the flow is stable. On the other hand, if the terminal shock occurs downstream a first jet cell, a change in the pressure surrounding the jet will influence the flow entering the shock and changes the position of the shock. Then the length of the jet varies and it affects the pressure in the recirculating region again.

Although the condition described above seems to be correct, it is necessary to clear the relationship between the length of the jet and the pressure in the recirculating region in order to obtain the critical value of the transition. Finley's attempt against it has resulted in failure because of his inviscid flow model as described in the previous section. Thus it is necessary to take the viscosity of fluid into account to predict the critical value of the transition. Due to the complexity of the phenomena in the viscous flow, only the Navier-Stokes simulation seems to be a useful means to estimate the pressure in the recirculating region.

18

As is mentioned above, a few flow models are suggested for the three types of region respectively, but all of them are insufficient to explain the oscillatory phenomena of the opposing jet flow. In the present study the author would like to use a method of numerical experiment in which the governing equations of fluid are solved to obtain the time-varying flow field. The detail of the numerical experiment used here will be described in next chapter.

19

Chapter 3   Numerical experiments

In this chapter the author will discuss the numerical experiments carried out in the present study, which contains topics of a modeling of the flow field, a computational method and its various results. Recently the Navier-Stokes simulation of a variety of complex flow fields has been a practical tool for fluid dynamics mainly because of great improvements of differential schemes such as ones called total variation diminishing schemes.[36-39] A large number of studies including computations of steady or unsteady flow fields have been published so far and achieved considerable successes. The author here uses one of the established computational techniques and obtains various properties of sequential flow fields in time.

3.1 Simplification of flow field

It has been indicated in the previous experiments that the actual oscillating flow field over a hemispherical nose with an opposing jet is not always axially symmetrical in spite of the employment of an axisymmetric model without angle of attack. Instantaneous schlieren photographs have revealed that the configuration of bow shock is considerably asymmetric about the axis of the model especially in the unstable case. If one wish to obtain the actual flow field using a method of numerical simulations, three-dimensional equations of motion of fluid is indispensable in the present problem for the reason described above. However it is not easy to analyze the unsteady three-dimensional solutions obtained by the same reason as

for the results of wind tunnel measurements. Thus the author will use an axisymmetric flow model in the present study on the hypothesis that the essential mechanism of oscillations of an opposing jet can be explained in the axisymmetric flow theory. This approach also allows us to save the computational time. In fact, the time-averaged flow patterns of the oscillating flow field are seen to be axially symmetrical as shown in Figure 2.5.

Former researchers have often used inviscid flow models to compute the flow field of the opposing jet.[11, 12, 35, 40] It was mainly due to the economical reason, but as a result of that they could not obtain successful results for the flow field in the unstable region. The author has found by preliminary computations that both the viscous and the inviscid models give the nearly same solution for the stable flow, but their solutions are mutually much different for the unstable flow.[41] It indicates the necessity of the viscous model for the unstable flow. Consequently, the viscous model may be needed to estimate the pressure in the recirculating region precisely.

Generally we can not ignore the turbulence in the analysis of the high Reynolds number flow. In this case the Reynolds number is so high that it is satisfactory to consider that the returning jet flow and the recirculating flow are fully turbulent. However the results of the numerical experiment as described below imply that the turbulent effect is slightly responsible to only the recirculating region. In fact the frequency of the oscillations of this problem is much lower than that of the usual turbulent fluctuations of free jets[42-44] and it has been showed by the previous investigations of the free jet that the jet boundary in the vicinity of the jet exit remains laminar.[45]

Thus it is assumed that the turbulence effect controls the attachment of the separated jet flow and the flow in the recirculating region, but do not directly affect the oscillations of the flow field. Under the above assumptions, the author will use no turbulent model in the present study in which the equation of viscous fluid will be directly solved without any artificial treatments involving the turbulent effects.

3.2 Numerical method

Governing equations

The governing equations for viscous compressible flows are the Navier-Stokes equations. In the present study, the simplified form of the equations will be adopted according to the assumption of the axisymmetric flow model. The derivation from the original three-dimensional form is described in appendix A in detail. The final form of the equations that are nondimensionalized and transformed to general curvilinear coordinates are

$$\frac{\partial \hat{Q}}{\partial t} + \frac{\partial \hat{F}}{\partial \xi} + \frac{\partial \hat{G}}{\partial \eta} + \hat{H} = \frac{1}{Re}\left(\frac{\partial \hat{F}_v}{\partial \xi} + \frac{\partial \hat{G}_v}{\partial \eta} + \hat{H}_v\right) \tag{3.1}$$

where $\hat{H}$ and $\hat{H}_v$ are axisymmetric source terms and Re is the Reynolds number based on the free stream condition and the reference length. Each vector in both members is expressed as

$$\hat{Q} = \frac{1}{J}\begin{pmatrix} \rho \\ \rho u \\ \rho v \\ e \end{pmatrix} \tag{3.2}$$

22

$$\hat{F} = \frac{1}{J}\begin{pmatrix} \rho U \\ \rho u U + \xi_x p \\ \rho v U + \xi_r p \\ (e+p)U \end{pmatrix}, \quad \hat{G} = \frac{1}{J}\begin{pmatrix} \rho V \\ \rho u V + \eta_x p \\ \rho v V + \eta_r p \\ (e+p)V \end{pmatrix}, \quad \hat{H} = \frac{1}{J}\begin{pmatrix} \rho v/r \\ \rho u v/r \\ \rho v^2/r \\ (e+p)v/r \end{pmatrix}$$

$$\hat{F}_v = \frac{1}{J}\begin{pmatrix} 0 \\ \xi_x \tau_{xx} + \xi_r \tau_{xr} \\ \xi_x \tau_{xr} + \xi_r \tau_{rr} \\ \xi_x \beta_x + \xi_r \beta_r \end{pmatrix}, \quad \hat{G}_v = \frac{1}{J}\begin{pmatrix} 0 \\ \eta_x \tau_{xx} + \eta_r \tau_{xr} \\ \eta_x \tau_{xr} + \eta_r \tau_{rr} \\ \eta_x \beta_x + \eta_r \beta_r \end{pmatrix}, \quad \hat{H}_v = \frac{1}{J}\begin{pmatrix} 0 \\ \tau_{xr}/r \\ \tau_{rz}/r \\ \beta_r/r \end{pmatrix}$$

where U and V are the contravariant velocities given as

$$U = \xi_x u + \xi_r v, \qquad V = \eta_x u + \eta_r v \tag{3.3}$$

and the metrics and the Jacobian J are given as

$$\xi_x = J r_\eta, \qquad \xi_r = -J x_\eta, \qquad \eta_x = -J r_\xi, \qquad \eta_r = J x_\xi \tag{3.4}$$

$$\frac{1}{J} = x_\xi r_\eta - x_\eta r_\xi$$

The stress and heat flux terms in the viscous fluxes are expressed as

$$\tau_{xx} = \frac{1}{3}\mu\left\{ 4\left(\xi_x u_\xi + \eta_x u_\eta\right) - 2\left(\xi_r v_\xi + \eta_r v_\eta\right) - \frac{2v}{r} \right\} \tag{3.5}$$

$$\tau_{rr} = \frac{1}{3}\mu\left\{ 4\left(\xi_r v_\xi + \eta_r v_\eta\right) - 2\left(\xi_x u_\xi + \eta_x u_\eta\right) - \frac{2v}{r} \right\}$$

$$\tau_{xr} = \mu\left(\xi_r u_\xi + \eta_r u_\eta + \xi_x v_\xi + \eta_x v_\eta\right), \qquad \tau_{rz} = 2\mu\left(\xi_r v_\xi + \eta_r v_\eta - \frac{v}{r}\right)$$

$$\beta_x = u\tau_{xx} + v\tau_{xr} + \frac{\mu}{Pr(\gamma-1)}\left(\xi_x c^2{}_\xi + \eta_x c^2{}_\eta\right)$$

$$\beta_r = u\tau_{xr} + v\tau_{rr} + \frac{\mu}{Pr(\gamma-1)}\left(\xi_r c^2{}_\xi + \eta_r c^2{}_\eta\right)$$

23

For the present flow condition, the air is assumed to have constant specific heats and obey the state equation of perfect gas as

$$p = \rho R T \qquad (3.6)$$

Solution algorithm

These equations are solved by a finite difference method and unsteady solutions are obtained at each time step through the time marching procedure. The modified Lax-Wendroff type explicit TVD (Total Variation Diminishing) scheme proposed by Yee[46, 47] is used to solve the discretized equations. The author has applied the scheme to several problems[15, 34, 41] so far and obtained remarkable successes in each case. This scheme is temporally and spatially second-order accurate and is suitable for the unsteady problem like this as well as steady ones.

The original scheme developed by Yee is applied to one-dimensional nonlinear systems and it is necessary to extend it to the multidimensional scheme in order to apply to the axisymmetric Navier-Stokes equations used here. Preserving the original second order time accuracy, the extension can be accomplished by either a predictor-corrector, Runge-Kutta multistage or Strang type of fractional step method. In the present study, a second order Runge-Kutta method is adopted for the time integration. Using the method, Yee's scheme can be implemented for the convective terms of governing equations as follows:

$$\hat{\boldsymbol{Q}}^* = \hat{\boldsymbol{Q}}^n + \mathcal{L}\left(\hat{\boldsymbol{Q}}^n\right) \qquad (3.7)$$

$$\hat{\boldsymbol{Q}}^{n+1} = \hat{\boldsymbol{Q}}^n + \frac{1}{2}\left(\mathcal{L}(\hat{\boldsymbol{Q}}^n) + \mathcal{L}(\hat{\boldsymbol{Q}}^*)\right)$$

24

where $\mathcal{L}$ is the operator for TVD differencing as

$$\mathcal{L}(\hat{\boldsymbol{Q}}_{j,k}) = -\Delta t\left(\tilde{\boldsymbol{F}}_{j+1/2,k} - \tilde{\boldsymbol{F}}_{j-1/2,k}\right) - \Delta t\left(\hat{\boldsymbol{G}}_{j,k+1/2} - \hat{\boldsymbol{G}}_{j,k-1/2}\right) \qquad (3.8)$$

with the grid spacing $\Delta\xi$ and $\Delta\eta$ being unit. The functions $\tilde{\boldsymbol{F}}_{j+1/2,k}$ and $\hat{\boldsymbol{G}}_{j,k+1/2}$ are the numerical fluxes in the ξ- and η-directions evaluated at $(j+1/2,k)$ and $(j,k+1/2)$, respectively. Typically, $\tilde{\boldsymbol{F}}_{j+1/2}$ (omitting the index for η-directions) for a non-MUSCL approach can be expressed as

$$\tilde{\boldsymbol{F}}_{j+1/2} = \frac{1}{2}\left(\hat{\boldsymbol{F}}_j + \hat{\boldsymbol{F}}_{j+1} + \boldsymbol{R}_{j+1/2}\boldsymbol{\Phi}_{j+1/2}\right) \qquad (3.9)$$

where $\boldsymbol{R}_{j+1/2}$ is the matrix whose columns are eigenvectors of flux Jacobian $\partial\hat{\boldsymbol{F}}/\partial\hat{\boldsymbol{Q}}$. The l-th element of the vector $\boldsymbol{\Phi}_{j+1/2}$ is

$$\Phi^l = -\Delta t\left(\Lambda^l\right)^2\Omega^l - \Psi(\Lambda^l)\left(\Lambda^l - \Omega^l\right) \qquad (3.10)$$

where Λ^l is the l-th eigenvalue of $\partial\hat{\boldsymbol{F}}/\partial\hat{\boldsymbol{Q}}$ and Λ is the difference vector of the characteristic variables in the local ξ-direction denoted, for example, as

$$\Lambda_{j+1/2} = \boldsymbol{R}^{-1}_{j+1/2}\left(\hat{\boldsymbol{Q}}_{j+1} - \hat{\boldsymbol{Q}}_j\right) \qquad (3.11)$$

The function $\Psi(z)$ of an entropy correction to $|z|$ is expressed as

$$\Psi(z) = \begin{cases} |z| & ; \; |z| \ge \delta \\ \dfrac{z^2 + \delta^2}{2\delta} & ; \; |z| < \delta \end{cases} \qquad (3.12)$$

where δ should be a function of the contravariant velocity and the corresponding sound speed for the blunt body computations. The form of the function used here is

$$\delta = \tilde{\delta}\left(|U| + |V| + c\sqrt{\xi_x^2 + \xi_r^2 + \eta_x^2 + \eta_r^2}\right) \qquad (3.13)$$

25

with a constant $\bar{\delta}$ setting to 0.1.

It is indicated that problems containing strong shock waves are sensitive to the treatment of limiter functions Ω^l. Several types of the form of the limiter functions are suggested by Yee. Using the more compressive limiter turns out to be more accuracy in terms of shock resolution than other more diffusive ones, but they have a low stability and very restricted time step limit. According to preliminary computations for the opposing jet problem, only the most diffusive limiter of them has been found to be free of unphysical solutions. The form is expressed as

$$\Omega^l_{j+1/2} = min\,mod\left[A^l_{j-1/2}, A^l_{j+1/2}\right] + min\,mod\left[A^l_{j+1/2}, A^l_{j+3/2}\right] - A^l_{j+1/2} \quad (3.14)$$

where the minmod function is given as

$$min\,mod(x,y) = sgn(x) \cdot max\left\{0, min\left[|x|, y \cdot sgn(x)\right]\right\} \quad (3.15)$$

We have to solve the Riemann problem to obtain average state $\hat{Q}_{j+1/2}$ at each interface. Roe[48] has proposed a method for finding approximately such solutions. His idea is closely tied with the characteristic field decomposition method that is an effective approximate local decoupling of the nonlinear system and is widely used in CFD practical applications at the present stage. Only the final solutions are described here and see his original papers in detail. For the two-dimensional and axisymmetric equations for a perfect gas, the Roe averaged state can be obtained as

$$u_{j+1/2} = \frac{u_j + Du_{j+1}}{1+D}, \qquad v_{j+1/2} = \frac{v_j + Dv_{j+1}}{1+D} \quad (3.16)$$

26

$$H_{j+1/2} = \frac{H_j + DH_{j+1}}{1 + D}$$

with

$$D = \sqrt{\frac{\rho_{j+1}}{\rho_j}} \qquad (3.17)$$

Computational domain and grid system

Because the blunt body is embedded into a supersonic stream in this problem and primary flow features such as jet and recirculating region exist around the symmetrical axis, the interesting domain is limited to the region that is bounded by the bow shock and the hemispherical nose of the blunt body. Thus the physical domain for the present computation can be defined by the Cartesian coordinates (x, r) as shown in Figure 3.1.

The grid points for the discretized calculation are placed on the body fitting curvilinear coordinates (ξ, η) and a 130×130 computational gird used here are shown in Figure 3.2, where the circumferential direction ξ corresponds to the index j and the perpendicular direction η corresponds to the index k. The grid points are clustered exponentially in the η direction in the vicinity of the body surface. The minimum grid spacing at the body surface is given as the magnitude of 200 as cell Reynolds number whose reference length is the grid spacing. The grid points in the ξ direction are clustered in the jet exit region and the minimum spacing at the lip of the jet exit is nearly same magnitude of that at the body surface in the η direction. All solutions to be described later including the case without a jet have been obtained using the same computational grid so that it is not necessary to consider the influences by different grid systems.

<u>Boundary and initial conditions</u>

Before advancing the solutions to next time step, values of the dependent variables for points on the boundaries of computational domain must be specified for the numerical operator. The boundary conditions on each boundary of the computational domain as shown in Figure 3.3 are implemented numerically as follows:

The variables on the inflow boundary AB ($1 \le j \le j_{max}$, $k = k_{max}$) are fixed to free stream ones as

$$f_{k=k_{max}} = f_{\infty} \tag{3.18}$$

where f denotes the dependent variables ρ, ρu, ρv and e. On the outflow boundary BC ($j = j_{max}$, $2 \le k \le k_{max} - 1$), the variables are given by a linear extrapolation from internal grid points as

$$f_{j=j_{max}} = 2f_{j=j_{max}-1} - f_{j=j_{max}-2} \tag{3.19}$$

Those on the body surface CD ($j_{lip} \le j \le j_{max}$, $k = 1$) are given by no-slip, zero-pressure gradient and adiabatic wall conditions as

$$u_{k=1} = v_{k=1} = 0 \tag{3.20}$$

$$p_{k=1} = p_{k=2}$$

$$T_{k=1} = T_{k=2}$$

The values on the jet exit DE ($1 \le j \le j_{lip} - 1$, $k = 1$) are specified according to the jet exit condition as

$$f_{k=1} = f_j \tag{3.21}$$

28

On the symmetric axis E A $(j=1, 2 \le k \le k_{max}-1)$, zero-th order extrapolation is practical since the condition represents no-flux across the axis as

$$f_{j-1} = f_{j-2} \tag{3.22}$$

The initial condition corresponds to the impulsive start. The values on all inner grid points $(2 \le j \le j_{max}-1, 2 \le k \le k_{max}-1)$ are initialized to those of a free stream before a start of calculations as

$$f_{j,k} = f_{\infty} \tag{3.23}$$

3.3 Numerical results

Computational objective

As mentioned in chapter 1, the data of Karashima et al. is used as the experimental basis for the present study. The time-averaged pressure measurements on the body and ordinary schlieren photographs are available for the experimental versus computational comparisons. They have examined a variety of flow conditions in which the free stream Mach number is in the range of 1.5 to 3.0 and the jet exit Mach number is in the range of 1.0 to 2.0. Because the objective of this study is not to get a series of practical data but to solve the physical phenomena, the author here will carry out the numerical experiments on one case of them in which the free stream Mach number and the jet exit Mach number are 2.5 and 1.0, respectively.

29

The configuration of the model employed in the wind tunnel experiment is also used in the present study. The jet exit is placed on the stagnation point of the hemispherical nose and its diameter is equal to $1/10$ of the cylinder diameter. The flow parameters obey the condition of the experiment as shown in Table 2.

Table 2   Flow conditions

Free stream	Reynolds number	1,470,000
	Mach number	2.5
	Total temperature	294(K)
Opposing jet	Mach number	1.0
	Total temperature	294(K)
	Total pressure ratio	$0.491 \sim 1.633$

Comparisons with experimental data

Before going into the discussion of the oscillatory phenomena by use of numerical solutions, it is necessary to confirm the accuracy of the flow model used here by comparisons with the experimental results. If there would be any significant discrepancies between the time-averaged computational solutions and the experimental data, it seems to be quite meaningless to discuss the time-varying computational solutions. So the author will first make some comparisons between the time-averaged computational solutions and the available experimental data. For this purpose, computations of the flow field have been performed for six total pressure ratios $p_{0j} / p_{0\infty}$ = 0.491, 0.816, 0.968, 1.005, 1.036 and 1.633. For $p_{0j} / p_{0\infty}$ = 0.491, the total pressure in the jet reservoir is equal to the stagnation pressure behind the bow shock and the jet stops issuing from the orifice. It will be called *no jet case* subsequently. The flow field corresponds

to the unstable or the stable region defined in the previous chapter for $p_{0j} / p_{0\infty}$ = 0.816 or 1.633, respectively. The remainder $p_{0j} / p_{0\infty}$ = 0.968, 1.005 and 1.036 are together in the transitional region, that is, the flow field changes from unstable to stable between $p_{0j} / p_{0\infty}$ = 0.968 and 1.036 in the experimental result.

In the beginning, the author would like to show comparisons of the time-averaged flow fields in both cases of $p_{0j} / p_{0\infty}$ = 1.633 and 0.816. A series of numerical solutions that are obtained at very small intervals are averaged in time for a comparison since only the time-averaged flow field is available in ordinary schlieren photographs. Figure 3.4 illustrates the time-averaged density contours for $p_{0j} / p_{0\infty}$ = 1.633. The exposure time is enough longer than a period of oscillation of the flow field as is described later. In this figure, each of a bow shock and a Mach disk as well as a highly under-expanded jet cell is clearly resolved as a thick line where iso-contour lines are clustered. Comparing with the schlieren photograph as in Figure 2.1, those shapes and locations on the axis are found to agree quite well each other. The reattachment shock, however, cannot be seen apparently in the computed density contours. It may be due to the lack of grid points about the reattachment region. The author here points out that there seems to be a great possibility that the flow field is taken to be completely stable if only time-averaged observations of the flow field is available.

Figure 3.5 illustrates the time-averaged density contours for $p_{0j} / p_{0\infty}$ = 0.816. In this case the exposure time is equal to that of the actual schlieren photographs. Contrary to the former result, both bow shock and Mach disk are dimmed in the contours and there might be two weak bow shocks at first sight. This observation seems to agree with the schlieren

photograph as in Figure 2.5. The fact mentioned above may imply that in this case the bow shock and Mach disk oscillate in considerable large amplitude and a period of the oscillation is the similar order of the exposure time. Because if the period is much longer than the exposure time, oscillating shock waves should be clearly resolved like a stationary shock, whereas if the period is much shorter than the exposure time, oscillating shock waves should be equally diffused in a broad of the flow field.

Next the time-dependent results of the numerical experiment here will be presented. Figure 3.6(a) ~ (f) show variations of position of the bow shock on the axis up to 15 non-dimensional time at six total pressure ratios described above, respectively. A non-dimensional time corresponds to the time that is required for the sound in the free stream to go through the reference length. Thus it seems to be quite all right to consider that each solution has reached steady state within the present computational time. In the no jet case as shown in Figure 3.6(a), the bow shock has rapidly reached its converged position that agrees quite well with the experimental result (not shown). For $p_{0j} / p_{0\infty} = 0.816$ as shown in Figure 3.6(b), the bow shock oscillates intensely with a large amplitude. It appears to a nearly simple harmonic oscillation. The most forward position of the bow shock has reached up to 2.8 times of no jet one and the amplitude is 15% of the body diameter. Although neither frequency nor amplitude of the oscillation can be compared with the experimental data, it appears that this solution represents the oscillatory flow in the unstable region. For $p_{0j} / p_{0\infty} = 0.968$ as shown in Figure 3.6(c), the oscillation of the bow shock is more remarkable and rather irregular than last case. In this case, the amplitude is no longer constant and it may also contain other waves which have higher frequencies than normal mode of the oscillation. Numerical solutions

shown in Figure 3.6(d) and (e) which correspond to the cases of $p_{0j} / p_{0\infty} =$ 1.005 and 1.036, respectively appears to behave each other in the same manner. For a little while after starting computation, the bow shock oscillates intensely by similar way to the case of $p_{0j} / p_{0\infty} = 0.968$. The solutions, however, change to another type of oscillation in 5 or 6 non-dimensional time. The new type of oscillation is considerably different from former one. The amplitude is small as 2% of the model diameter and the frequency is rather higher than that of former one. This second type of oscillatory solution is also obtained by computing the flow field for $p_{0j} / p_{0\infty} = 1.633$ as shown in Figure 3.6(f). In this case, the large-amplitude type of oscillation does not appear even at the initial stage of a computation and the flow field becomes the small-amplitude type of oscillation as soon as the bow shock reaches its mean position. The magnitude of the amplitude is less than the width of the thick line representing a bow shock in the experimental photograph. Thus it is anticipated that we cannot find this small oscillation in ordinary schlieren photographs and this oscillatory solution corresponds to the small oscillation in the stable region described in chapter 2.

Comparisons of the surface pressure distribution between the time-averaged numerical solutions and the experimental data are shown in Figure 3.7(a) ~ (f). The values of pressure at grid points on the body surface obtained at every time steps are averaged in time during a few periods of the oscillation and the distribution is expressed by the solid line in these figures. The plateau-like pressure at the vicinity of the symmetrical axis denotes the jet exit pressure that is specified as the boundary condition according to each total pressure ratio. Considerable decrease in pressure around the jet occurs as a result of a large separation of the jet flow. As

shown in Figure 3.7(a), the agreement in the no jet case is excellent. In other cases, curves of the numerical results agree fairly well with the experimental data where the pressure decrease by a separation of the jet can be clearly represented although slight quantitative discrepancies exist around the reattachment point where the surface pressure has the maximum value because of an impingement of the jet flow. The cause of this discrepancy may be mainly due to the lack of grid points around the reattachment point so that the location of reattachment or the strength of the reattachment shock cannot be resolved in a correct manner.

Figure 3.8 shows the variation of the mean pressure in the recirculating region with the total pressure ratio, in which the pressure at the angle of 15 degree from the stagnation point is used as the typical pressure in the recirculating region to compare the experimental data. It is obvious at a glance from this figure that the decreasing pressure with total pressure ratio experiences an abrupt rise at certain total pressure ratio, which implies the transition of the flow field from the unstable region to the stable region. Although the computation slightly overestimates the pressure than the measurement in all cases of the total pressure ratio examined here, the tendency of the pressure variation agrees well each other, moreover, the transition occurs at nearly same total pressure ratio in both the computation and the experiment.

As a result of these comparisons, it has been proved that all features of the opposing jet flow observed by the experiments such as the existence of stable and unstable type of flow, the transition from one to another and the pressure decrease by a separation are clearly obtained from the numerical solutions. Therefore it can be considered that the accuracy of the simplified

flow model used assuming the axisymmetric flow is satisfactory for a way of resolving the phenomena of the opposing jet flow. The author will discuss the flow field in the stable and unstable region in detail in following sections.

Flow field in the stable region

In the previous investigations, only the steady analysis has been carried out on the flow field in the stable region. However it has been confirmed in the present numerical experiment that there is a small oscillation of the bow shock even in the region whose possibility of existence has been indicated by a few former researchers. In this section, the author will discuss the oscillatory numerical solutions in the stable region in detail.

As might be suspected from the flow field pattern in the stable region illustrated in chapter 2, if the bow shock oscillates, also the Mach disk and the free stagnation must oscillate. Figure 3.9 shows those oscillations as well as the bow shock on the symmetrical axis for $p_{0j} / p_{0\infty} = 1.633$. The author would like to mention here that in the present computation shock position at each step is defined as the location of the change of velocity across Mach 1.0 and the free stagnation is defined as the location of zero velocity. As shown in this figure, the oscillation of the Mach disk has the nearly same amplitude as that of the bow shock, but the amplitude of the oscillation of the free stagnation is up to about three times as that.

Figure 3.10(a) ~ (c) show the results of the spectrum analysis using FFT method on the time-variations of the positions of the free stagnation, the bow shock and the Mach disk, respectively. The frequency is non-dimensionalized by use of the sound speed in the free stream and the

reference length. A slight smoothing by a frequency filter is applied on the spectrum distribution obtained. The details of the FFT method used will be described in Appendix B.[49] Figure 3.10(a) shows that the power spectrum of oscillation of the free stagnation is discrete distribution and has several peaks whose non-dimensional frequencies are in increasing order 2.5, 5.0, 7.5, 10.0... . It is obvious on inspection from this result that the second and after frequencies are multiples of the first frequency, in other words, the oscillation of the free stagnation is a periodic one with harmonics. It may be also implies that the oscillation is not a simple harmonic one but a nonlinear one called relaxation oscillation. On the other hand, the power spectrum of oscillation of the bow shock and the Mach disk shown in Figure 3.10(b) and (c), respectively have also discrete distribution and are much similar each other. They also have the first and second peaks at the same frequencies as those of the free stagnation but higher harmonics are not apparent in these figures. These results seem to indicate that the oscillations of the bow shock and the Mach disk depend on the oscillation of the free stagnation that is regarded as an oscillation with one degree of freedom whose non-dimensional frequency of normal mode is about 2.5. Because the second or third normal mode must appear in the spectrum distribution if it is a strongly coupled oscillation with two or three degrees of freedom. Thus it is assumed that we can approximately solve this oscillation problem by considering only the oscillation of the free stagnation.

We can see many important features of the flow field such as shock waves, shear layers and separations by drawing density contours of the numerical solutions. Figure 3.11(a) ~ (h) show changes of the flow field during a period of the oscillation T_1 for $p_{0j} / p_{0\infty} = 1.633$. The interval of time between each figure is about 0.06. It is found from these figures that

36

the configuration of the bow shock is nearly constant through a period of the oscillation, but the jet structure rather changes in time. As is illustrated below, it is due to remarkable change of the pressure surrounding the jet. It is well known that the structure of a free jet depends on the surrounding pressure and alternative type of jet structure appears according to the pressure value.[45] When the surrounding pressure is much lower than the jet exit pressure, the barrel shock reflects on the symmetrical axis in the manner of the Mach reflection. Contrary, when the surrounding pressure is slightly lower than that, the barrel shock reflects in the manner of the regular reflection. The reason of the changes of the jet structure in the opposing jet flow can be explained by analogy with a free jet. However it must be emphasized here that the structure of an opposing jet in this case is always the type of the Mach reflection through a period of the oscillation, so that the flow on the axis is not affected by the pressure outside the jet. Consequently, the position of the Mach disk can be completely prescribed by the static condition of the opposing jet described in chapter 2. From the aforementioned point of view, we can readily understand that no large oscillation occurs in the stable region.

Now we have a question why the flow field is not completely stable at this total pressure ratio. It is satisfactory to consider that even if a small fluctuation occurs in the flow field by some reason, that can be readily damped by the viscosity of fluid. The answer associated with a new flow model will be presented in next chapter.

Flow field in unstable region

The larger oscillation of the flow field in the unstable region would more attract our attention due to its magnitude and the unknown

37

mechanism. In this section, the author will discuss the numerical solutions for $p_{0j} / p_{0\infty} = 0.816$ that represents a typical flow field in the unstable region in order to solve the mechanism of the oscillation. It may be the first to obtain a series of instantaneous flow fields in the unstable region that has been impossible by means of wind tunnel experiments.

Figure 3.12 illustrates the oscillation of the bow shock, the Mach disk and the free stagnation in the case of the unstable region. One thing that the author would like to mention here is that the supersonic jet in this case can contain more than two cells in itself and the Mach disk means the terminal shock in the final cell through which the jet flow decelerates to subsonic flow. It is indicated by this figure that the oscillations of both the Mach disk and the free stagnation appear to be nearly simple harmonic as well as the bow shock and the magnitudes of their amplitudes are almost same value. Figure 3.13(a) ~ (c) show the results of the FFT analysis on the time-variation of the position of the free stagnation, the bow shock and the Mach disk, respectively. These figures show that each distribution of the power spectrum has a peak at the common non-dimensional frequency being about 0.9. It seems to be the strongest proof that the bow shock, the Mach disk and the free stagnation move together. However it is difficult to consider that this oscillation is an simple harmonic oscillation about a certain neutral position because the motions of the free stagnation and the Mach disk are much different from a sine curve and the amplitude is remarkable large. The above statement will be emphasized again in the discussion of the changes of the flow field described below.

Drawing density contours of the numerical solutions at various time steps will give us extremely useful information especially on the unsteady

38

flow field. Figure 3.14(a) ~ (h) show changes of the flow field during a period of the oscillation T_2 for $p_{0j} / p_{0\infty} = 0.816$. The interval of time between each figure is about 0.16. A sequence of the figures starts from the stage when the jet length that is here defined by the location of the Mach disk is shortest in a period as in Figure 3.14(a). At this moment, a supersonic opposing jet terminates through a nearly normal shock (Mach disk) and immediately lose its total pressure until the value of the free stagnation. The situation is similar to the flow field for $p_{0j} / p_{0\infty} = 1.633$. As the time goes on, the structure of the first cell of the jet changes to the regular reflection type and the second cell of the jet appears following the first cell as shown in Figure 3.14(b) ~ (c). As a result, the jet length gradually increases so that both the bow shock and the free stagnation also go forward although the position of the free stagnation cannot be discernible in the density contours. At this phase, the jet flow experiences a pair of oblique shocks in the first cell until terminating by a normal shock in the second cell, then the longer distance is required to lose fully its total pressure until the value of the free stagnation. In Figure 3.14(d), an abrupt transition of the shock structure in the first cell occurs where the regular reflection of the barrel shocks changes to the Mach reflection. In a while, the diameter of the Mach disk increases and the entire flow after the Mach disk becomes subsonic, so that the Mach disk at the end of the second cell disappears as in Figure 3.14(e). The disappearance of the Mach disk in the second cell means the breakdown of the second cell at the same time that is clearly visible in Figure 3.14(f). Then the jet length is suddenly shortened so that the bow shock and the free stagnation also begin going back toward the most backward position as shown in Figure 3.14(g). At this time, the vorticities generated from the jet boundary of the broken second jet cell flows downstream. Consequently, the length of the first jet cell decreases

39

till the original one at the end of a period and the nearly same shape of the jet reappears as in Figure 3.14(h).

As is described above, the flow field in the unstable region experiences remarkable changes of the jet structure during a period of the oscillation. There appears two different types of jet structure in turn. One type has a short jet cell terminating by a normal shock and the other has two cells where the first cell contains oblique shocks reflection and the second cell contains a normal shock as well as the former type. It is satisfactory to consider that this oscillation of the bow shock, the Mach disk and the free stagnation is actually the transitional motion between two different equilibrium states. This assumption will be explained in detail in the next chapter.

Chapter 4   Development of flow models

Remembering the objectives of the present study, it was to clarify the mechanism of oscillatory phenomena in the opposing jet flow and to develop physical models representing the mechanism. At the present stage, we have obtained a variety of results of the numerical experiments here. The author will in this chapter develop some new models of the flow fields in the stable, unstable and transitional region on bases of the numerical solutions.

4.1 Stable region

Equilibrium state

In the stable region, a few former researchers have already developed flow models in equilibrium state as described in chapter 2. The author will suggest a more accurate model of the equilibrium flow field on basis of the numerical solutions. The density contours of the time-averaged flow field in the stable region have been already presented in Figure 3.4. The author here emphasizes the pattern of jet flow and the recirculating region by drawing jet stream lines and subsonic region as in Figure 4.1. It is clear from this figure that the jet flow turns back after decelerating to subsonic and produces a low speed recirculating region between the jet and the body surface. This result proves schematically the flow patterns illustrated in the previous flow models such as in Figure 2.2 and 2.3. Figure 4.2 shows a new flow model developed in the present study by use of a variety of results of numerical experiments described above. Although the outline of this model is very similar to previous ones, the structure of a jet is especially

emphasized here. It is illustrated from the density contours that the supersonic flow passing the barrel shock and the reflected shock emanating the triple point is decelerated to subsonic flow by a terminal shock at last. There is subsonic pocket around the symmetrical axis bounded by the bow shock, the Mach disk and the terminal shock. The nearly still fluid in the subsonic pocket begins to flow downstream along the jet boundary and is accelerated to supersonic again. It is satisfactory to consider that the present model explains actual phenomena precisely as far as stable flow field. The static condition of the opposing jet developed by Romeo is naturally applied on this model and the location of the Mach disk on the axis can be determined by simple calculations.

Instability of flow field

In spite of a more accurate flow model above, we have never still obtained any interpretation about the small oscillation of the shock waves and the free stagnation in the stable region whose existence has been indicated in the present numerical experiment as well as the previous measurements. Therefore the author will here attempt to develop an oscillatory flow model in the stable region. The model is based on the one-dimensional inviscid theory of fluid dynamics and will explain the mechanism of oscillation of the shock waves and the free stagnation on the symmetrical axis.

We are going to back to the Romeo's one-dimensional model as in Figure 2.4 and start from there in order to construct an oscillatory model. It seems to be clear in his model that the system of the bow shock, the free stagnation and the Mach disk remains still if no fluctuation occurs in the system. Assuming that a small fluctuation such as slight disturbances of

42

the free stream or jet flow occur in the system for some reason, what happens in the system? We will at first assume the occurrence of a small fluctuation of the free stagnation because the assumption is not considered to lose generality in this problem. If the free stagnation moves slightly upstream in the jet flow, in other words, towards the jet exit, a weak compressive pressure disturbance will propagate toward the Mach disk and an expansive pressure disturbance with the same magnitude as former will propagate toward the bow shock as shown in Figure 4.3. Each pressure disturbance Δp propagates in a subsonic region at a speed of $\bar{c} - \bar{u}$, where $\bar{c}$ and $\bar{u}$ denote the mean speed of sound and the mean speed of fluid in the subsonic region, respectively. When the pressure disturbance Δp reaches the bow shock, it causes the bow shock to move at the velocity according to the formula[50] as

$$\dot{x}_b = k_1 \Delta p \tag{4.1}$$

where $\dot{x}_b$ denotes the bow shock velocity in the upstream direction of free stream and k_1 is a positive function of free stream Mach number that can be assumed to be constant here. It is readily found that if the pressure disturbance is compressive ($\Delta p > 0$), the bow shock moves upstream in the free stream, and if the pressure disturbance is expansive ($\Delta p < 0$), the bow shock moves downstream. In this case, the bow shock moves downstream and stops after the free stagnation stops. We can here ignore the speed of the motion of shock waves because it is rather smaller than that of the free stream. Thus the quasi-steady analysis will be applied subsequently. Consequently the motion of the bow shock fully depends on the fluctuation of the free stagnation while the free stagnation will not be affected by the motion of the bow shock.

On the other hand, it is not the same situation in the case of the Mach disk. When the pressure disturbance Δp reaches the Mach disk, it causes the Mach disk to move at the velocity according to the above mentioned formula as

$$\dot{x}_d = k_2 \Delta p \qquad (4.2)$$

where $\dot{x}_d$ denotes the Mach disk velocity in the upstream direction of jet flow and k_2 is a positive function of Mach number ahead of the Mach disk that depends on the location of Mach disk as described in chapter 2. After upstream motion of the Mach disk due to an incoming compressive pressure disturbance, the Mach number ahead of the Mach disk decreases so that the strength of the Mach disk also decreases. It means at the same time that the total pressure just behind the Mach disk increases. It is assumed here that the increment of total pressure behind the Mach disk is in proportion to the displacement of the Mach disk under the assumption of a small displacement. Then the increment of the total pressure is given as

$$\Delta p'_{0j} = k_3 x_d \qquad (4.3)$$

where $\Delta p'_{0j}$ denotes the increment of the total pressure behind the Mach disk and x_d denotes the displacement of the Mach disk in upstream direction. The positive value k_3 is assumed to be constant regarding to the location of the Mach disk and expressed as

$$k_3 = \left. \frac{\partial p'_{0j}}{\partial x} \right|_{x = x_d} \qquad (4.4)$$

where $p'_{0j} = p'_{0j}(x)$ is the total pressure distribution behind the Mach disk on the symmetric axis, which is for example given in Eq. (2.2).

44

The total pressure increment behind the Mach disk means the increment of the velocity of fluid just behind the Mach disk. Thus the increment of total pressure $\Delta p'_{0j}$ is in this time transferred downstream as the increment of the mean flow velocity $\bar{u}$ in the subsonic region. When the total pressure disturbance reaches the free stagnation, the free stagnation, strictly speaking, the fluid at the free stagnation suffers a force due to the imbalance static pressure between both sides of it. The magnitude of the force working upon the fluid of unit volume is equal to the incoming total pressure disturbance and the force works downstream in the jet flow because of the incoming positive pressure disturbance. It indicates that the fluid at the free stagnation suffers the force whose direction is opposite to that of initial displacement of the free stagnation. In this case the force will work upon the fluid at the free stagnation downstream in the jet flow if the initial displacement occurs upstream. Consequently, it is found that the fluid at the free stagnation suffers the recovery force against its displacement, in other words, it is the system of statically stable.

Generally a system of an oscillation suffers damping forces as well as recovery forces. If some positive damping forces works upon the system, any fluctuations in the system gradually disappear in time. The present numerical experiment, however, has showed that the small oscillation of the flow field in the stable region remains for a computational time. The fact is in agreement with the results of the previous measurements. The author will in this time discuss the damping force working upon the system of the oscillation.

The fluid at the free stagnation does not suffer the recovery force simultaneously with its displacement because the pressure disturbance due

to a displacement of the free stagnation goes around the subsonic region until returning to itself. The time lag T_c required for a traveling disturbance is given approximately as

$$T_c = \frac{l}{\bar{c} - \bar{u}} + \frac{l}{\bar{u}} \tag{4.5}$$

where l denotes the distance between the free stagnation and the Mach disk. The existence of the time lag implies that the free stagnation has already proceeded for some distance when the disturbance returns. Assuming that the velocity of the free stagnation $\dot{x}_{st}$ is constant for time T_c, the effective displacement of the free stagnation that causes the recovery force can be given as $x_{st} - \dot{x}_{st} T_c$, where x_{st} is the actual displacement of the free stagnation. Therefore the equation of motion of the fluid of mass m at the free stagnation can be expressed in the limitation of the inviscid theory as

$$m\ddot{x}_{st} + \Delta p'_{0j} = 0 \tag{4.6}$$

where $\Delta p'_{0j}$ can be given according to the above discussion as

$$\Delta p'_{0j} = k_3 \alpha (x_{st} - \dot{x}_{st} T_c) \tag{4.7}$$

where α is introduced as a positive factor that gives the ratio of the magnitude of displacement of the free stagnation to the magnitude of displacement of the Mach disk. If the Mach disk moves same distance as the free stagnation, α can be set to unit. Consequently, the equation of motion of the fluid at the free stagnation is reexpressed as

$$m\ddot{x}_{st} - k_3 \alpha T_c \dot{x}_{st} + k_3 \alpha x_{st} = 0 \tag{4.8}$$

46

It is readily found that this equation has a negative damping coefficient since the values k_3, α and T_c are positive. Therefore it is concluded that the system is dynamically unstable and tends to occur a self-excited oscillation with ease. In many mechanical and electrical systems, time lag or retarded actions are the essential feature that produces self-excited oscillations.[51]

Although an oscillatory flow model applied to the small oscillation in the stable region has been developed above, the author would like to emphasize here that the present model treats only the initial stage of the actual oscillation under a linear theory. It can be considered that the actual damping force is a non-linear function of the amplitude so that the damping coefficient can become positive as the amplitude increases. As a result, the oscillation will enter a limit cycle and the amplitude will converge to a finite magnitude.

Feedback mechanism

We have obtained the formula as Eq. (4.8) that demonstrates the instability of the free stagnation that also brings the motion of the bow shock and the Mach disk. The oscillatory model above, however, treats only the motion of them on the symmetric axis and ignores the change of the surrounding flow field that is illustrated in Figures 3.11(a) ~ (h). In this section, the author will discuss the two-dimensional feedback mechanism sustaining the small oscillation in the stable region.

The motion of the free stagnation on the axis means at the same time the change of location of the contact surface between the free stream and the jet flow. As is anticipated from the flow field in Figure 4.1, it affects the shape of the recirculating region so that the pressure in the region will

47

change considerably. The fact has been indicated by Finley[8] and will be also presented as the results of numerical experiment here in later section. Consequently the variation of the pressure in the recirculating region influences the shape of the jet boundary and the barrel shock in the opposing jet as is illustrated in Figures 3.11(a) ~ (h). The jet flow on the axis entering the Mach disk is not affected by the change of the barrel shock, whereas the flow passing both the barrel and the reflected shock depends strongly on the configuration of the shocks and the jet boundary. That is, the pressure disturbance originated in the recirculating region can be propagated into the subsonic region behind the Mach disk through the circumferential region of the jet containing the barrel and reflected shocks. The pressure disturbance changes the static pressure in the subsonic region and influences the location of the Mach disk. Then the motion of the Mach disk causes the motion of the free stagnation in the manner as shown in the one-dimensional oscillatory model described before.

As is described above, it is anticipated that actual propagation of the pressure disturbance from the free stagnation to the Mach disk is not in a straight manner on the axis, which has been described in the one-dimensional model, but in a winding manner through the recirculating region. It is, however, noted that the same explanation as the former one-dimensional model can be applied for the occurrence of the oscillation since the similar time lag due to a traveling disturbance exists in this two-dimensional feedback system. Consequently it is satisfactory to consider that the small oscillation in the stable region occurs and is sustained according to the mechanism of this model. Future measurements of the frequency of the oscillation in the stable region are necessary to demonstrate the validity of the present oscillatory model.

4.2 Unstable region

It has been showed in chapter 2 that the Fox's flow model in the unstable region may contain serious contradictions. The reason of Fox's failure seems to be omitting the changes of the jet structure. In this chapter, the author will suggest a new flow model that can explain accurately the mechanism of the oscillation in the unstable region. It is based on the free jet theory in which the structure of a jet changes with the surrounding pressure.

Feedback mechanism

As is described in chapter 3, the present numerical experiment has exhibited drastic changes of the structure of the jet in which alternative type of the shock reflection appears in turn inside the first cell of the jet and temporally second cell of the jet extends the jet length. It is generally known that any self-excited oscillations require some feedback mechanism. The author will discuss the feedback mechanism of the oscillation.

We can see the changes of the recirculating region in time associated with the location of the free stagnation by drawing a series of instantaneous stream lines as in Figures 4.4(a) ∼ (h). These figures have been obtained simultaneously with Figures 3.18(a) ∼ (h), respectively. They clearly illustrate that the recirculating region expands as the free stagnation advances, and contracts as it goes back. From the facts described above, it can be stated that the motion of the free stagnation, in other words, the variation of the jet length changes the volume of the recirculating region so that it may change the pressure in the region.

49

We have now discussed the influence of the change of the jet length on the surrounding pressure. Contrary, it is possible to know the influence of the change of the surrounding pressure on the jet length using the fruits of a large number of investigations of free jets. Love et al.(1959)[52] have made experimental and theoretical studies of axisymmetric free jets in detail. They have investigated the effects of jet Mach number, nozzle divergence angle and jet static pressure ratio upon jet structure, jet wavelength and the shape and curvature of the jet boundary for jets exhausting into still air. Figure 4.5 shows the effect of static pressure ratio p_j / p_∞ upon non-dimensional primary wavelength w/d that denotes the length of the first cell of a jet over the jet exit diameter. It is found from the results that the length of the first jet cell increases with the static pressure ratio.

However it is more important in the results of Love et al. that the abrupt change of the pattern of the shock reflection inside a jet occurs at the static pressure ratio of 2 in the case of jet exit Mach number of 1.0. It implies that the jet structure changes from the Mach reflection type to the regular reflection type as the surrounding pressure increases over a half of the jet exit pressure that is assumed to be constant. What happens on an opposing jet after this remarkable change of the jet structure? It is well known that the loss of a total pressure through a shock wave depends on the strength of the shock. It gives the maximum value for a normal shock and decreases as the shock wave inclines to the direction of flow. Therefore when the barrel shock reflects on the symmetrical axis in the Mach reflection type, the jet flow passing the Mach disk will lose enough amount of total pressure for satisfying the static condition of an opposing jet and the jet terminates just after the Mach disk. On the other hand, when the barrel shock reflects on the axis in the regular reflection type, the jet flow suffers

much less loss of total pressure than the flow passing a normal shock. This amount of the total pressure loss is so insufficient for consisting with the static condition that the jet flow remains supersonic and a following second cell appears. From the statements described above, it can be concluded that the variation of the pressure surrounding the jet changes the structure of the first cell of the jet and controls the appearance of the second cell so that changes the total length of the jet drastically.

In order to examine the feedback mechanism described above, the author will show the motion of the free stagnation and the variation of the pressure surrounding the jet that are derived from the numerical solution for $p_{0j} / p_{0x} = 0.816$ in Figure 4.6. It is clear from this figure that both oscillations have the same period and the nearly opposite phase. That is, the surrounding pressure has its maximum value just after the position of the free stagnation is most backward, while the surrounding pressure has its minimum value just after the position of the free stagnation is most forward. Here the author would like to show the critical surrounding pressure at which a jet structure changes from the regular reflection type to the Mach reflection type. The non-dimensional surrounding pressure p_s / p'_{0x} is expressed as

$$\frac{p_s}{p'_{0x}} = \frac{p_{0x}}{p'_{0x}} \cdot \frac{p_{0j}}{p_{0x}} \cdot \frac{p_s}{p_{0j}} \tag{4.9}$$

where the second fraction means the total pressure ratio that is equal to 0.816 in this case. The first fraction denotes the total pressure ratio across a normal shock that is given by the well-known formula[53] as

51

$$\frac{p_{0\infty}}{p'_{0\infty}} = \frac{\left(\frac{2\gamma}{\gamma+1} M_\infty^2 - \frac{\gamma-1}{\gamma+1}\right)^{\frac{1}{\gamma-1}}}{\left(\frac{\frac{\gamma+1}{2} M_\infty^2}{1 + \frac{\gamma-1}{2} M_\infty^2}\right)^{\frac{\gamma}{\gamma-1}}} \tag{4.10}$$

Also the third fraction can be reexpressed using the isentropic relation[53] as

$$\frac{p_s}{p_{0j}} = \frac{1}{\left(1 + \frac{\gamma-1}{2} M_j^2\right)^{\frac{\gamma}{\gamma-1}}} \cdot \frac{p_s}{p_j} \tag{4.11}$$

Substituting Eq. (4.10) and (4.11) into Eq.(4.9) and using the critical pressure ratio of Love et al. ($p_j / p_s = 2$), the non-dimensional surrounding pressure can be obtained. A dashed line in the figure represents the threshold of the transition between the Mach reflection and the regular reflection. The Mach reflection occurs under the line, while the regular reflection occurs over the line. It is clear from this figure that in this case the jet structure must change one type to another type in turn during a period of the oscillation.

Oscillation cycle

Taking the feedback mechanism described above into consideration, the author will develop the cycle of the oscillation in the unstable region as illustrated in Figure 4.7(a) ~ (d). We will start the short jet phase for convenience as in Figure 4.7(a) in which the bow shock locates most backward position in a period and the recirculating region gives the minimum volume. At the beginning of this phase, there is only a first cell of the jet that contains a normal shock at the end. At this time the pressure in the recirculating region that means the pressure surrounding jet gives the maximum value that is more than the threshold of the change of the jet

52

structure as shown in Figure 4.7(b). Therefore the structure of the first jet cell rapidly changes to the regular reflection type that is generally called *slightly under-expanded jet*, so that a second cell appears ahead of the first cell as in Figure 4.7(c). This means that the length of the jet that is defined the distance from the jet exit to the free stagnation increases in time. The free stagnation finally reaches its most forward position and the length of the jet gives the maximum value at the same time. At this phase, if the pressure value in the recirculating region might be consistent with the jet structure, the flow would become stable. However the long jet including two cells enlarges the recirculating region and reduces the pressure in that region. As a result, the pressure surrounding the jet may become less than the threshold of the change of the jet structure and the structure of the first jet cell changes to the Mach reflection type that is called *highly under-expanded jet* as shown in Figure 4.7(d). After this change occurs, the flow passing the Mach disk in the first cell cannot remain supersonic so that the second cell of the jet disappears at once. The free stagnation now rapidly goes back, namely, the length of the jet decreases in time. Finally the length of the jet gives its minimum value again, where the volume of the recirculating region is also minimum as shown in Figure 4.7(a). The changes of the flow field repeat in this cycle.

Amplitude of oscillation

As is described above, we have now obtained the flow model that can explain qualitatively the mechanism of the oscillation in the unstable region. The quantitative problems, however, have been still left unsolved such as the frequency or the amplitude of the oscillation. Although the prediction of the frequency of the oscillation is the subject for a future study, the amplitude of the oscillation can be given approximately by use of

an analogy with free jets. The author will mention the amplitude of the oscillation in this section.

Reconsidering the flow model described above, when the length of the jet gives its maximum value, the jet consists of a first cell containing oblique shocks and a second cell containing a Mach disk. On the other hand, when the length of the jet gives its minimum value, the jet consists of only a first cell containing a Mach disk. As is indicated in the free jet theory, the jet consisting of oblique shock cells gives an iterative structure then it is considered that physical properties at the end of the first cell are nearly same ones at the jet exit. It is assumed from this fact that the length of the second cell of the Mach reflection type at the long jet phase is nearly same as that of the first cell at the short jet phase. The numerical solution described in chapter 3 confirms the above assumption. Therefore it is satisfactory to consider that the amplitude of oscillation of the opposing jet that is expressed as the difference between the maximum jet length and the minimum jet length is equal to the length of the first cell at the long jet phase.

As is described before, Love et al. have showed the results of measurements of the length of the first cell as in Figure 4.5. They have also developed semiempirical relations to predict experimental values under the fact that abrupt change of the jet structure from the regular reflection to the Mach reflection occurs at the pressure ratio of 2. Their two formulas on the length of a first jet cell w are given as[52]

$$\frac{w}{d} = 1.55 \sqrt{M_j{}^2 \left(\frac{p_j}{p_\infty}\right) - 1} - 0.55\beta_j \qquad ; \ \frac{p_j}{p_\infty} \le 2 \qquad (4.12)$$

54

$$\frac{w}{d} = 1.52\left(\frac{p_j}{p_\infty}\right)^{0.437} + 1.55\left(\sqrt{2M_j^2 - 1} - 1\right)$$
$$- 0.55\beta_j + 0.5\left[\frac{1}{1.55}\sqrt{\left(\frac{p_j}{p_\infty} - 2\right)\beta_j} - 1\right] \quad ; \quad \frac{p_j}{p_\infty} > 2 \tag{4.13}$$

where

$$\beta_j = \sqrt{M_j^2 - 1} \tag{4.14}$$

and M_j is the jet exit Mach number. Eqs. (4.12) and (4.13) correspond to the regular reflection and the Mach reflection, respectively. The curve given by these equations is shown by the solid line in Figure 4.5 and gives a good prediction of the experimental results.

It is necessary to estimate the static pressure ratio p_j / p_∞ for obtaining the length of the first jet cell using above formulas. Although it is naturally possible by use of the pressure in the recirculating region derived from the numerical solution, the way seems to be meaningless because the numerical solution also gives the length of the first jet cell as well as the pressure in the recirculating region. The author would rather like to evaluate the static pressure ratio by no use of solutions of large-scale computations.

Considering the above requirement, the author would like to emphasize here that the long jet phase appears just after the change of the jet structure from the regular reflection to the Mach reflection. Moreover it is indicated in the experimental results that the change occurs at the static pressure ratio of 2. Therefore assuming that the maximum jet length realizes at the same time as the change of the jet structure, the length of the first cell of the jet with maximum length that is considered to be the

amplitude of oscillation can be obtained by substituting $p_j / p_\infty = 2$ into the formula giving the length of the first jet cell. The result of this simple prediction in the case of jet exit Mach number of 1.0 and the present numerical experiment as described in chapter 3 are given in Table 3.

Table 3   Amplitude of large oscillation in unstable region

Theoretical prediction	$1.55d$
Numerical experiment	$1.50d$

The agreement between both values is quite well. Consequently it may be quite all right to consider that a simple method of prediction of the amplitude suggested here is also sufficiently accurate method. Figure 4.8 shows the amplitude of the oscillation in the unstable region predicted by the present method as a function of the jet exit Mach number. It clearly indicates that the amplitude increases with the jet exit Mach number. The author emphasizes the point that the amplitude of the oscillation depends on only the jet exit Mach number regardless of the free stream Mach number and the total pressure ratio under the conditions of the unstable flow. Naturally the condition of the unstable flow depends on both the free stream Mach number and the total pressure ratio. The confirmation of the results for cases except the jet exit Mach number of 1.0 is the subject for a future study.

4.3 Transitional region

In previous sections the author has developed flow models in the stable and unstable region and predicted frequency or amplitude of those oscillations. It is, however, very important to clear the condition of the

transition between the stable and the unstable region for complete understanding of the opposing jet flow. As is described in chapter 2, Finley has suggested a condition for the transition. The main point of the condition is that the transition occurs at the total pressure ratio in which the jet terminal shock according to the static condition of the opposing jet locates at the same position on the axis as the first intersection of barrel shock in an equivalent free jet whose surrounding pressure is equal to that in the recirculating region. In this section, the author will prove quantitatively the validity of the condition of Finley and discuss the effects of the Mach number of free stream and jet on the threshold of transition.

Condition of transition

In order to discuss the Finley's condition, it is necessary to obtain preliminarily the location of the shock intersection on the axis as well as that of the Mach disk as a function of the total pressure ratio. Love et al. have also measured the variation of location of the intersection of the barrel shock on the axis inside a first jet cell. Figure 4.9 shows the non-dimensional distance from the plane of the jet exit to the focal point of the intersecting shock for the jet exit Mach number of 1.0. The distance s/d increases with increasing p_j/p_∞ as would be expected. In case of the opposing jet flow, it is necessary to use the pressure in the recirculating region as the surrounding pressure p_∞ in order to determine the distance s/d from this figure. It is possible by using the results of the viscous numerical computations here.

Figure 4.10(a) ~ (e) show the time-histories of the pressure in the recirculating region during a few periods for five total pressure ratios. The pressure in the recirculating region is derived here from the surface

pressure in vicinity of jet exit lip. The pressure tends to oscillate considerably in time for all cases. In the unstable flow case of $p_{0j} / p_{0\infty} =$ 0.816 and 0.968 as in Figure 4.10(a) and (b), respectively, there are very steep peaks of the pressure that are due to the impingement of the broken jet on the body surface. In other portion of the time-history, the variation of the surrounding pressure is rather moderate. On the other hand, in the stable flow case of $p_{0j} / p_{0\infty} =$ 1.005, 1.036 and 1.633 as in Figure 4.10(b), (c) and (d), respectively, the each oscillation of the surrounding pressure has nearly constant amplitude and no abrupt peak exists. The steep increase of the pressure is due to the shock impingement on the body, whereas the gradual decrease after that is due to the expansion wave impingement.

These figures also contain the threshold of transition of the shock reflection in the first jet cell, which can be evaluated in the same manner as that in last section. Each dashed line represents the threshold under which the Mach reflection exists while over which the regular reflection is realized. In the unstable flow case, the surrounding pressure varies across the threshold so that both types of reflection appear in a period (in the case of $p_{0j} / p_{0\infty} =$ 0.816 it has been already shown in Figure 4.6). Contrary, in the stable flow case the surrounding pressure is under the threshold in almost portion of a period, namely, only the Mach reflection appears during a period. This statement corresponds well the results of observations of the computed density contours in chapter 3.

By use of the surrounding pressure derived from numerical solutions and the jet exit pressure specified according to the jet reservoir pressure, the non-dimensional distance from jet exit plane to the intersection of barrel shock can be readily obtained from Figure 4.9. It is noted that the static

pressure ratio p_j / p_s can be obtained from the non-dimensional surrounding pressure $p_s / p'_{0\infty}$ using Eqs. (4.9) ~ (4.11) again. Moreover the distance from jet exit plane to the Mach disk required for the static condition with the total pressure ratio can be also obtained from Eq. (2.3). As is described above, the surrounding pressure oscillates intensely in all cases, so that a simple average of each maximum and minimum values is employed for the present estimation.

Figure 4.11 gives the calculated distances to intersecting shock with the total pressure ratio appending the curve that represents the variation of the distance to the Mach disk by which the jet terminates. As in this figure, the location of the intersecting shock agrees that of the Mach disk at the total pressure ratio $p_{0j} / p_{0\infty}$ = 0.968. Above the value of $p_{0j} / p_{0\infty}$, the distance to intersecting shock is larger than that to Mach disk so that the incoming flow to the Mach disk is not affected by anyone. On the other hand, below the value of $p_{0j} / p_{0\infty}$, the barrel shocks intersect on the axis before the Mach disk so that the expanding flow terminates on the intersecting point. As the result, a second jet cell is required before the terminal Mach disk. If the Finley's idea as described in chapter 2 is applied, it is anticipated that the flow field becomes stable above the total pressure ratio of $p_{0j} / p_{0\infty}$ = 0.968. This prediction agrees quite well with the numerical experiment here as well as the experimental result. Therefore it is satisfactory to say that the Finley's static condition has quantitatively proved to give the threshold of transition between the stable and the unstable region.

Effects of Mach number

The author would like to mention here the effects of the Mach number of a free stream and a jet flow on the threshold of transition. The experimental results are used for this aim since the computational results included in the present study are of only a pair of both Mach numbers. Figure 4.12 shows the variation of the threshold of transition with a free stream Mach number and a jet exit Mach number. It is found that the threshold decreases as a free stream Mach number increases under the constant jet exit Mach number. It seems to be explained as follows: The increment of free stream Mach number results in strengthening a bow shock so that the total pressure behind the shock decreases. The reduction of total pressure behind the bow shock means at the same time the reduction of pressure in the recirculating region, so that the static pressure ratio of the jet increases and the distance to intersecting shock becomes larger. Therefore the smaller total pressure ratio is required for giving the same location for the Mach disk and the intersecting shock that satisfies the condition of transition.

On the other hand, Figure 4.12 also illustrates that the increase of the jet exit Mach number results in the increase of the total pressure ratio of the threshold. The increase of the jet exit Mach number means the large reduction of the pressure at jet exit plane since reservoir pressure is constant, so that the static pressure ratio of jet decreases. As a result, the distance to the intersecting shock decreases and the larger total pressure ratio is required for giving the same location for the Mach disk and the intersecting shock that satisfies the condition of transition.

60

In summary, the Mach number of the free stream and the issuing jet affect the jet static pressure ratio so that the location of the intersecting shock is influenced, while the location of the Mach disk is also slightly affected by the change of both Mach numbers. The location of the Mach disk is a weak function of the free stream Mach number as is obvious from Eqs. (2.3) and (2.4), but its variation may be rather smaller than that of the location of intersecting shock. Moreover the change of location of the Mach disk is small unless the very high jet exit Mach number since the Mach number distribution on the axis is nearly same except in the vicinity of the jet exit regardless of the jet exit Mach number.[28] Therefore it is satisfactory to consider that the effect of both Mach numbers is mainly to change the location of the intersecting shock so that to change the total pressure ratio of the threshold that satisfies the condition of transition. The author thinks that this effect of the Mach number can be quantitatively demonstrated by the computations as well as the experiments. It is, however, beyond the range of the present study.

It has been indicated in this chapter that the feedback mechanisms that are indispensable for self-sustained oscillations exist in both the stable and unstable flow field. The author here summarizes the feedback mechanism in the oscillatory opposing jet flow in Figure 4.13 on the basis of the discussion until now. It is apparent in the figure that the path for a traveling signal is identical for the stable and unstable flow in the most part of the feedback cycle. Only the way for a signal to go from the location of the intersecting shock to the location of the Mach disk is different between the stable region and the unstable region. In the stable region the change of the shape of the intersecting shock affects the flow field behind Mach disk, whereas in the unstable region it affects the flow field in front of Mach disk.

It is the reason for the difference of the magnitude of Mach disk motion between the stable and the unstable flow. That is, changes of the flow in front of the Mach disk have greater influence on the motion of the Mach disk than that of the flow behind it. Then a signal propagates in either way according to the condition of transition.

Chapter 5   Concluding remarks

Some flow models that explain the mechanism of oscillations of an opposing jet from a hemispherical nose have been developed in the present study. To obtain unsteady flow fields, a series of numerical experiments assuming the axisymmetric flow have been carried out. Based on the analysis of the numerical solutions and the previous experimental results, the following conclusions are drawn:

- The present numerical experiments have successfully reproduced the oscillations of the stable and the unstable region as well as the transition between both regions. The time-averaged pressure on the body and the threshold of transition agree quantitatively with the measured data.

- In the stable region, the feedback mechanism of a small disturbance containing the time lag exists in the system of the free stagnation and the Mach disk. Therefore the system is statically stable and dynamically unstable so that the self-excited oscillation about its neutral position tends to occur.

- In the unstable region, the changes of the jet structure and the pressure in the recirculating region work as the feedback mechanism, so that the drastic oscillation of the bow shock, Mach disk and the free stagnation occurs between two possible equilibrium states. The amplitude of this large oscillation can be analogically obtained from the length of a first cell of the corresponding free jet.

- In the transitional region, it has been quantitatively proved that Finley's static condition represents the condition of the transition between the stable and the unstable region. The effect of the Mach number of a free stream and an issuing jet on the threshold of the transition is mainly to change the jet static pressure ratio so that to change the location of the intersecting shock on the axis.

The author expects that a new path has opened in the research of the oscillatory opposing jet flow by the present study. The numerical experiments obtaining time-dependent solutions can be a powerful tool for investigating the unsteady flow field like this. The author is also convinced that the truth of the present flow models will be demonstrated by further studies.

Bibliography

[1] Charczenko, N. and Hennessey, K.W., *Investigation of a Retrorocket Exhausting from the Nose of a Blunt Body into a Supersonic Free Stream*, NASA TN D-751 (1961).

[2] Lopatoff, M., *Wingflow study of pressure drag reduction at transonic speed by projecting a jet of air from the nose of a prolate spheroid of fineness ratio of 6*, NASA RM L51E09 (1951).

[3] Love, E.S., *The effects of a small jet of air exhausting from the nose of a body of revolution in supersonic flow*, NASA RM L52I19a (1952).

[4] Warren, C.H.E., *An experimental investigation of the effect of ejecting a coolant gas at the nose of a bluff body*, Journal of Fluid Mechanics, **8** : 400-417 (1960).

[5] Watts, G.A., *An experimental investigation of a sonic jet directed upstream against an uniform supersonic flow*, UTIA TN 7 (1956).

[6] Hayman, L.O., Jr., *Jet Effects on Cylindrical Afterbodies Housing Sonic and Supersonic Nozzles which Exhaust against a Supersonic Stream at Angles of Attack from 90° to 180°*, NASA TN D-1016 (1962).

[7] Romeo, D.J. and Sterret, J.R., *Exploratory investigation of the effect of a forward facing jet on the bow shock of a blunt body in a Mach number 6 free stream*, NASA TN D-1605 (1963).

[8] Finley, P.J., *The flow of a jet from a body opposing a supersonic free stream*, Journal of Fluid Mechanics, **26** (part 2) : 337-368 (1966).

[9] Karashima, K. and Sato, K., *An Experimental Study of an Opposing Jet*, Bulletin of ISAS, **11** (1A) : 53-64 (1975).

[10] Karashima, K. and Sato, K., *Personal communication*, (1992).

[11] Hirose, N. and Kawamura, R., *Numerical Calculation of Supersonic Opposing Jet Directed Upstream against Supersonic Main Stream by the Use of Time-Differece Method*, Proceedings of 9th ISTS-Tokyo : 311-317 (1971).

[12] Satofuka, N. and Matsuno, N., *Numerical Calculation of the Interaction between Opposing Jets and Supersonic Free Stream*, Journal of Japan Society for Aeronautical and Space Sciences, **23** (262) : 586-595 (1975).

[13] Macaraeg, M., *Application of CFD to Aerothermal Heating Problems*, AIAA paper 86-0232 (1986).

[14] Fox, J.H., *Counterflow Sonic Nosejet into a Supersonic Stream*, AIAA paper 86-1808 (1986).

[15] Fujita, M. and Kubota, H., *A Simulation of Flow Separation Effects ahead of Blunt Bodies*, Proceedings of 4th ISCFD-Davis : 359-364 (1991).

[16] Hartmann, J. and Lazarus, F., *The Air-Jet with a Velocity exceeding that of Sound*, Philosophical Magazine, **31** : 35-50 (1939).

[17] Pack, D.C., *On the Formation of Shock-Waves in Supersonic Gas Jets (Two-Dimensional Flow)*, The Quarterly Journal of Mechanics and applied Mathmatics, **1** : 1-17 (1947).

[18] Pack, D.C., *A Note on Prandtl's Formula for the Wave-Length of a Supersonic Gas Jet*, Quarterly Journal of Mechanics and Applied Mathematics, **3** (Part 2) : 173-181 (1949).

[19] Ladenburg, R., Voorhis, C.C.V. and Winckler, J., *Interferometric Studies of Faster than Sound Phenomena (Part 2:Analysis of Supersonic Air Jets)*, The Physical Review, **76** (2) : 662-677 (1949).

[20] Wilcox, D.E. and Weir, A., Jr., *Location of Mach Discs and Diamonds in Supersonic Air Jets*, Journal of the Aeronautical Sciences, **24** (2) : 150-157 (1957).

[21] Love, E.S., *An Approximation of the Boundary of a Supersonic Axisymmetric Jet Exhausting Into a Supersonic Stream*, Journal of the Aeronautical Sciences, **25** (2) : 130-131 (1958).

[22] Mikhail, A.G., Hankey, W.L. and Shang, J.S., *Computation of a Supersonic Flow Field Past an Axisymmetric Nozzle Boattail with Jet Exhaust*, AIAA paper 78-993 (1978).

[23] Tam, C.K.W. and Jackson, J.A., *A multiple-scales model of the shock-cell structure of imperfectly expanded supersonic jets*, Journal of Fluid Mechanics, **153** : 123-149 (1985).

[24] Kim, Y.N., Buggeln, R.C. and McDonald, H., *Computation of Multi-Dimensional Viscous Supersonic Jet Flow*, NASA CR 4020 (1986).

[25] Abdol-Hamid, K.S. and Wilmoth, R.G., *Multiscale Turbulence Effects in Supersonic Jets Exhausting Into Still Air*, NASA TP 2707 (1987).

[26] Abdol-Hamid, K.S., *Development of Three-Dimensional Code for the Analysis of Jet Mixing Problem*, NASA CR 4200 (1988).

[27] Owen, P.L. and Thornhill, C.K., *The flow in an Axially-Symmetric Supersonic Jet from a Nearly-Sonic Orifice into a Vacuum*, Aeronautical Research Council Reports and Memoranda 2616 (1952).

[28] Adamson, T.C., Jr. and Nicholls, J.A., *On the Structure of Jets From Highly Underexpanded Nozzles Into Still Air*, Journal of the Aero/Space Sciences, **26** (16) : 16-24 (1959).

[29] Ashkenas, H. and Sherman, F.S., *The Structure and Utilization of Supersonic Free Jets in Low Density Wind Tunnels*, in *Rarefied Gas Dynamics* : 84-105, ACADEMIC PRESS (1966).

[30] Romeo, D.J. and Sterrett, J.R., *Flow Field for Sonic Jet Exhausting Counter to a Hypersonic Mainstream*, AIAA Journal, **3** (3) : 544-546 (1965).

[31] Cassanova, R.A. and Wu, Y.C.L., *Flow Field of a Sonic Jet Exhausting Counter to a Low-Density Supresonic Airstream*, The Physics of Fluids, **12** (12) : 2511-2514 (1969).

[32] Mair, W.A., *Experiments on Separation of Boundary Layers on Probes in Front of Blunt-Nosed Bodies in a Supersonic Air Stream*, Philosophical Magazine, **43** (342) : 695-716 (1952).

[33] Maull, D.J., *Hypersonic flow over axially symmetric spiked bodies*, Journal of Fluid Mechanics, **8** (Part 4) : 584-592 (1960).

[34] Fujita, M., *Numerical Simulation of Flowfield over a Spiked Blunt-Nose*, Computational Fluid Dynamics Journal, **1** (2) : 187-195 (1992).

[35] Nishida, M., Teshima, K., Ueno, K. and Tanaka, S., *Shock Waves Generated by an Opposing Jet*, Proceedings of 17th ISSS-Bethlehem : 114-119 (1989).

[36] Yee, H.C. and Kutler, P., *Application of Second-Order-Accurate Total Variation Diminishing (TVD) Schemes to the Euler Equations in General Geometries*, NASA TM 85845 (1983).

[37] Young, V.Y.C. and Yee, H.C., *Numerical Simulation of Shock Wave Diffraction by TVD Schemes*, AIAA paper 87-0112 (1987).

[38] Yee, H.C., Warming, R.F. and Harten, A., *Implicit Total Variation Diminishing (TVD) Schemes for Steady-State Calculations*, Journal of Computer Physics, **57** (3) : 327-360 (1985).

[39] Yee, H.C. and Harten, A., *Implicit TVD Schemes for Hyperbolic Conservation Laws in Curvilinear Coordinates*, AIAA paper 85-1513 (1985).

[40] Hirose, N., *Computer Experiment of Supersonic Opposing Jet by a Time-Dependent Finite-Difference Method*, Proceedings of 10th ISTS-Tokyo : 497-504 (1973).

[41] Fujita, M. and Kubota, H., *Numerical Simulation of Opposing Jet from Hemisphere-Nose*, Proceedings of 18th ISTS-Kagoshima : 799-804 (1992).

[42] Powell, A., *On the Mechanism of Choked Jet Noise*, Proceedings of The Physical Society-Section B-: 1039-1056 (1953).

[43] Hammitt, A.G., *The Oscillation and Noise of an Overpressure Sonic Jet*, Journal of the Aerospace Sciences, **28** (9) : 673-680 (1961).

[44] Tam, C.K.W., Seiner, J.M. and Yu, J.C., *Proposed Relationship between Broadband Shock Associated Noise and Screech Tones*, Journal of Sound and Vibration, **110** (2) : 309-321 (1986).

[45] Kawamura, R., *Study on Axially Symmetric Supersonic Jets with Special Regard to the Shock Waves in Them*, Report of Institute of Science and Technology, **6** (3) : 141-148 (1952).

[46] Yee, H.C., *Upwind and Symmetric shock-capturing schemes*, NASA TM 89464 (1987).

[47] Yee, H.C., *A Class of High-Resolution Explicit and Implicit Shock-Capturing Methods*, NASA TM 101088 (1989).

[48] Roe, P.L., *Approximate Riemann Solvers, Parameter Vectors and Difference Schemes*, Journal of Computer Physics, **43** (2) : 357-372 (1981).

[49] Childers, D.G., *IEEE PRESS Selected Reprint Series: Modern Spectrum Analysis*, IEEE PRESS (1978).

[50] Karashima, K., *Instability of Shock Wave on Thin Airfoil in High Subsonic Flow*, Aeronautical Research Institute Report 363 (1961).

[51] Harris, C.M. and Crede, C.E., *Shock and Vibration Handbook*, McGraw-Hill Book Company, Inc. (1961).

[52] Love, E.S., Grigsby, C.E., Lee, L.P. and Woodling, M.J., *Experimental and Theoretical Studies of Axisymmetric Free Jets*, NASA TR R-6 (1959).

[53] The Staff of the Ames 1- by 3- foot Supersonic Wind-Tunnel section, *Notes and Tables for Use in the Analysis of Supersonic Flow*, NACA TN 1428 (1947).

[54] Pulliam, T.H. and Steger, J.L., *Recent Improvements in Efficiency, Accuracy and Convergence for Implicit Approximate Factorization Algorithms*, AIAA paper 85-0360 (1985).

Appendix A   Axisymmetric Navier-Stokes equations

The Cartesian coordinated three-dimensional Navier-Stokes equations in non-dimensional and strong conservation law form are written as

$$\frac{\partial \boldsymbol{Q}}{\partial t} + \frac{\partial \boldsymbol{E}}{\partial x} + \frac{\partial \boldsymbol{F}}{\partial y} + \frac{\partial \boldsymbol{G}}{\partial z} = \frac{1}{Re}\left(\frac{\partial \boldsymbol{E}_v}{\partial x} + \frac{\partial \boldsymbol{F}_v}{\partial y} + \frac{\partial \boldsymbol{G}_v}{\partial z}\right) \tag{A.1}$$

where

$$\boldsymbol{Q} = \begin{pmatrix} \rho \\ \rho u \\ \rho v \\ \rho w \\ e \end{pmatrix}, \quad \boldsymbol{E} = \begin{pmatrix} \rho u \\ \rho u^2 + p \\ \rho uv \\ \rho uw \\ (e+p)u \end{pmatrix}, \quad \boldsymbol{F} = \begin{pmatrix} \rho v \\ \rho uv \\ \rho v^2 + p \\ \rho vw \\ (e+p)v \end{pmatrix}, \quad \boldsymbol{G} = \begin{pmatrix} \rho w \\ \rho uw \\ \rho vw \\ \rho w^2 + p \\ (e+p)w \end{pmatrix} \tag{A.2}$$

$$\boldsymbol{E}_v = \begin{pmatrix} 0 \\ \tau_{xx} \\ \tau_{yx} \\ \tau_{zx} \\ \beta_x \end{pmatrix}, \quad \boldsymbol{F}_v = \begin{pmatrix} 0 \\ \tau_{xy} \\ \tau_{yy} \\ \tau_{zy} \\ \beta_y \end{pmatrix}, \quad \boldsymbol{G}_v = \begin{pmatrix} 0 \\ \tau_{xz} \\ \tau_{yz} \\ \tau_{zz} \\ \beta_z \end{pmatrix}$$

The components of the stress tensor and heat flux vector are given by

$$\tau_{xx} = -\frac{2}{3}\mu\left(u_x + v_y + w_z\right) + 2\mu u_x \tag{A.3}$$

$$\tau_{yy} = -\frac{2}{3}\mu\left(u_x + v_y + w_z\right) + 2\mu v_y$$

$$\tau_{zz} = -\frac{2}{3}\mu\left(u_x + v_y + w_z\right) + 2\mu w_z$$

$$\tau_{xy} = \tau_{yx} = \mu\left(u_y + v_x\right) \qquad \tau_{xz} = \tau_{zx} = \mu\left(u_z + w_x\right) \qquad \tau_{yz} = \tau_{zy} = \mu\left(v_z + w_y\right)$$

71

$$\beta_x = u\tau_{xx} + \upsilon\tau_{xy} + w\tau_{xz} + \frac{\mu}{Pr(\gamma-1)}c^2{}_x$$

$$\beta_y = u\tau_{yx} + \upsilon\tau_{yy} + w\tau_{yz} + \frac{\mu}{Pr(\gamma-1)}c^2{}_y$$

$$\beta_z = u\tau_{zx} + \upsilon\tau_{zy} + w\tau_{zz} + \frac{\mu}{Pr(\gamma-1)}c^2{}_z$$

These original equations are firstly transformed to the cylindrical coordinates (x',r,θ,t') in order to establish the final axisymmetric form. From the views shown in Figure A1, the relationship between the Cartesian and cylindrical coordinates are

$$x = x' \tag{A.4}$$

$$y = r\cos\theta$$

$$z = r\sin\theta$$

$$t = t'$$

and partial derivatives in the Cartesian coordinate are also transformed as

$$\frac{\partial}{\partial x} = \frac{\partial}{\partial x'} \tag{A.5}$$

$$\frac{\partial}{\partial y} = \cos\theta\,\frac{\partial}{\partial r} - \frac{\sin\theta}{r}\frac{\partial}{\partial\theta}$$

$$\frac{\partial}{\partial z} = \sin\theta\,\frac{\partial}{\partial r} + \frac{\cos\theta}{r}\frac{\partial}{\partial\theta}$$

$$\frac{\partial}{\partial t} = \frac{\partial}{\partial t'}$$

72

As a result, the cylindrical velocity components (u',v',w') are expressed as

$$u = u' \tag{A.6}$$

$$v = v' \cos\theta - w' r \sin\theta$$

$$w = v' \sin\theta + w' r \cos\theta$$

and for example, the partial derivative of v respect with y can be transformed to a slightly complex form as

$$v_y = v'_r \cos^2\theta + \left(2w' - rw'_r - \frac{v'_\theta}{r}\right) \sin\theta\cos\theta + \left(\frac{v'}{r} + w'_\theta\right) \sin^2\theta \tag{A.7}$$

Cartesian coordinates   Cylindrical coordinates
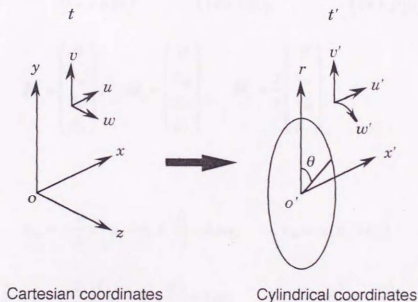
Figure A1   Coordinate transformation

Once all terms in the original equations are transformed, we can obtain the cylindrical coordinated Navier-Stokes equations (it is not shown here because of its much complex form). Then we can obtain the axisymmetric Navier-Stokes equations by letting

73

$$w' = \frac{\partial}{\partial \theta} = 0 \tag{A.8}$$

$$\theta = 0$$

and the resulting equations are

$$\frac{\partial \boldsymbol{Q}}{\partial t} + \frac{\partial \boldsymbol{F}}{\partial x} + \frac{\partial \boldsymbol{G}}{\partial r} + \boldsymbol{H} = \frac{1}{Re}\left(\frac{\partial \boldsymbol{F}_v}{\partial x} + \frac{\partial \boldsymbol{G}_v}{\partial r} + \boldsymbol{H}_v \right) \tag{A.9}$$

where

$$\boldsymbol{Q} = \begin{pmatrix} \rho \\ \rho u \\ \rho v \\ e \end{pmatrix}, \quad \boldsymbol{F} = \begin{pmatrix} \rho u \\ \rho u^2 + p \\ \rho u v \\ (e+p)u \end{pmatrix}, \quad \boldsymbol{G} = \begin{pmatrix} \rho v \\ \rho u v \\ \rho v^2 + p \\ (e+p)v \end{pmatrix}, \quad \boldsymbol{H} = \frac{1}{r}\begin{pmatrix} \rho v \\ \rho u v \\ \rho v^2 \\ (e+p)v \end{pmatrix} \tag{A.10}$$

$$\boldsymbol{F}_v = \begin{pmatrix} 0 \\ \tau_{xx} \\ \tau_{xr} \\ \beta_x \end{pmatrix}, \quad \boldsymbol{G}_v = \begin{pmatrix} 0 \\ \tau_{xr} \\ \tau_{rr} \\ \beta_r \end{pmatrix}, \quad \boldsymbol{H}_v = \frac{1}{r}\begin{pmatrix} 0 \\ \tau_{xr} \\ \tau_{rz} \\ \beta_r \end{pmatrix}$$

and

$$\tau_{xx} = -\frac{2}{3}\mu\left(u_x + v_r + \frac{v}{r} \right) + 2\mu u_x \qquad \tau_{xr} = \mu\left(u_r + v_x \right) \tag{A.11}$$

$$\tau_{rr} = -\frac{2}{3}\mu\left(u_x + v_r + \frac{v}{r} \right) + 2\mu v_r \qquad \tau_{rz} = 2\mu\left(v_r - \frac{v}{r} \right)$$

$$\beta_x = u\tau_{xx} + v\tau_{xr} + \frac{\mu}{Pr(\gamma-1)}c^2{}_x$$

$$\beta_r = u\tau_{xr} + v\tau_{rr} + \frac{\mu}{Pr(\gamma-1)}c^2{}_r$$

74

The above Cartesian coordinated Navier-Stokes equations are usually transformed to general curvilinear coordinates before the computation. The details can be seen in the previous publication[54], for example and the final expressions have been presented as Eq. (3.1) ~ (3.5) in chapter 3.

Appendix B   Spectrum analysis using FFT method

Considering a discrete time series x_j from $t = 0$ to $t = T$, which can be expressed as

$$x_j = x(j\Delta t) \quad ; j = 0,1,2,\dots,N-1 \tag{B.1}$$

where

$$\Delta t = \frac{T}{N}$$

and the number of data N is commonly set to n-th power of 2 as follows

$$N = 2^n \quad (n: \text{integer}) \tag{B.2}$$

Before Fourier transformation, the original time series is multiplied by a smooth function as the data window. A following cosine-bell-ended window seems to be reasonable.

$$W(t) = \frac{1}{2}\left(1 - \cos\frac{10\pi}{T}t\right) \qquad \text{for } 0 \le t \le \frac{1}{10}T \tag{B.3}$$

$$1 \qquad\qquad \text{for } \frac{1}{10}T \le t \le \frac{9}{10}T$$

$$\frac{1}{2}\left(1 - \cos\frac{10\pi}{T}(T-t)\right) \quad \text{for } \frac{9}{10}T \le t \le T$$

Then the complex Fourier transformation X_k can be calculated as

$$X_k = \sum_{j=0}^{N-1} x_j \, exp\left(-i2\pi\frac{k}{N}j\right)\frac{T}{N} \quad ; k = 0,1,2,\cdots,\frac{N}{2} \tag{B.4}$$

and the raw power spectrum is derived from X_k as

$$\tilde{P}_X\left(\frac{k}{T}\right) = \frac{\Delta t}{N}\left(A_k^2 + B_k^2\right) \tag{B.5}$$

where

$$X_k = A_k + iB_k$$

The result must be corrected in a following way if one has used any type of smooth window.

$$\tilde{P}_X \rightarrow \mu \tilde{P}_X \tag{B.6}$$

where

$$\mu = \frac{1}{0.875}$$

if the window function of Eq.(B.3) is used. It is recommended that the spectrum obtained is modified by a smoothing filter since the raw power spectrum often demonstrates considerable oscillations especially in higher frequency region. For example, the following triangular filter is used for this aim.

$$\hat{P}_X\left(\frac{k}{T}\right) = \frac{1}{l^2}\sum_{j=-l+1}^{l-1}\left(l-|j|\right)\tilde{P}_X\left(\frac{k-j}{T}\right) \tag{B.7}$$

where l is the number of terms of smoothing filter in frequency domain, that is, the larger l produces the more diffusive spectrum distribution.
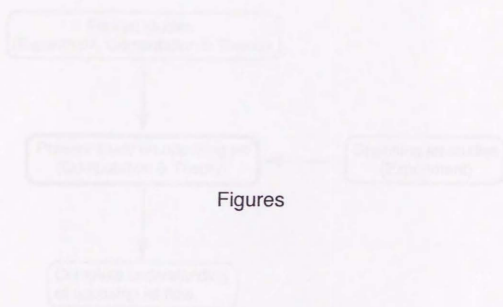
Figures
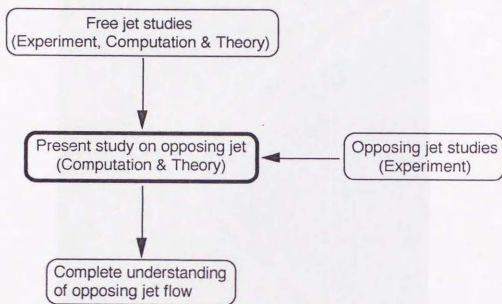
Figure 1.1   Schematic approach in the present study
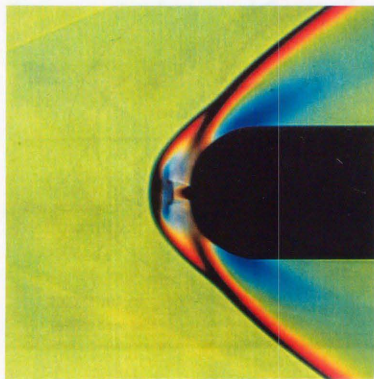
Figure 2.1   Schlieren photograph for $p_{oj}/p_{o\infty} = 1.633$ [10]
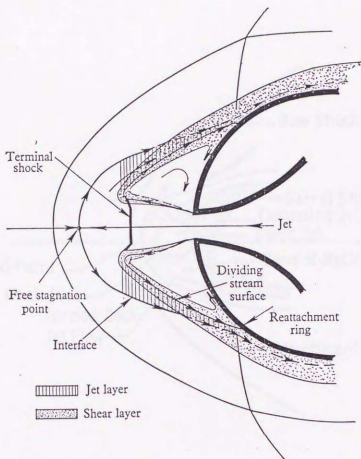
Figure 2.2   The flow model of Finley in the stable region[8]
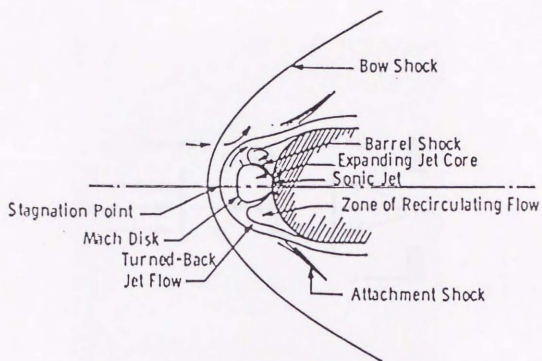
Figure 2.3   The flow model of Fox in the stable region[14]
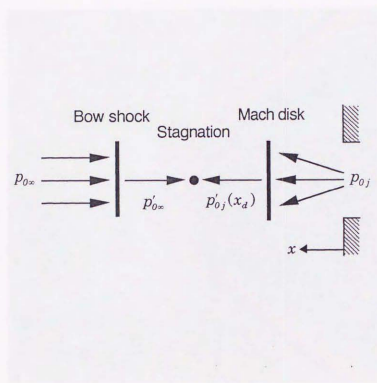
Figure 2.4   One-dimensional equilibrium flow model[7]
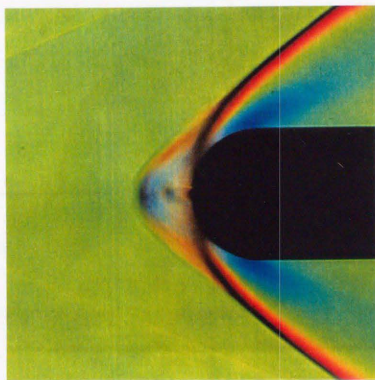
Figure 2.5   Schlieren photograph for $p_{0j}/p_{0\infty} = 0.816$ [10]
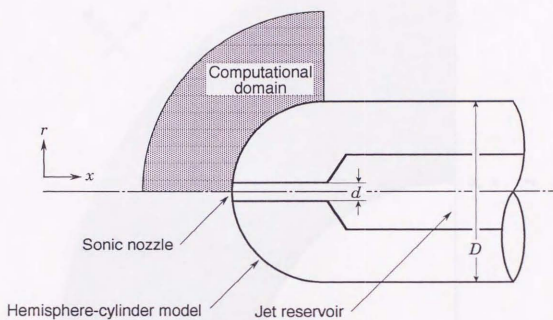
Figure 3.1   Computational domain
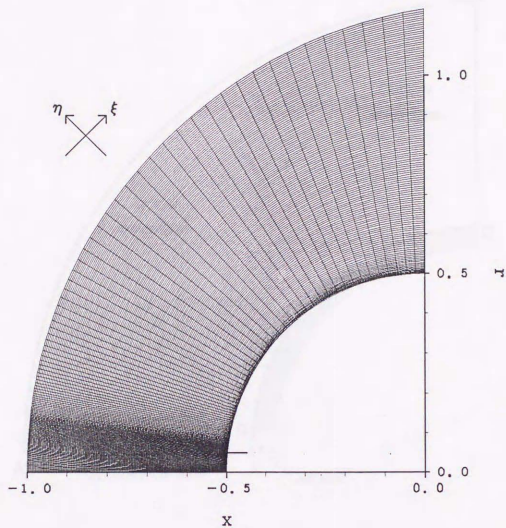
Figure 3.2　A 130×130 computational grid
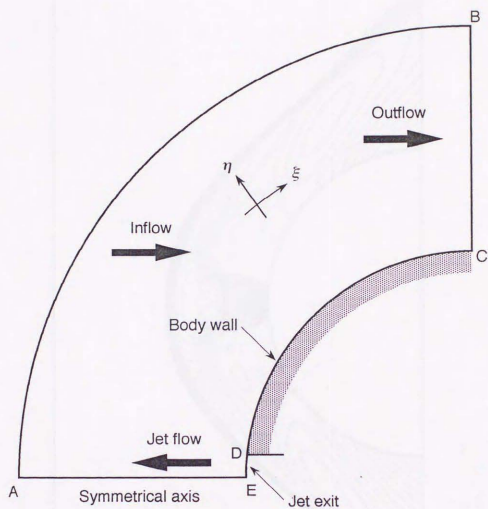
Figure 3.3 Boundary conditions
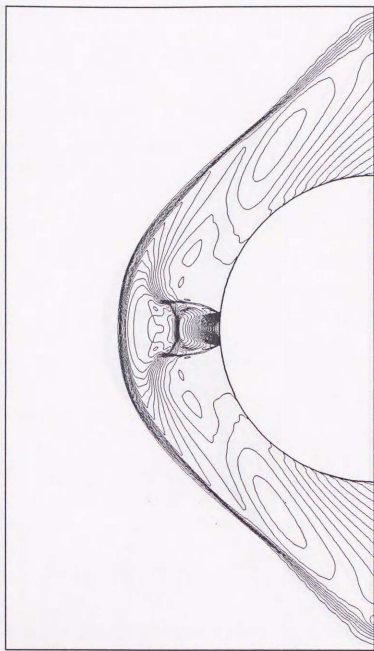
Figure 3.4   Time-averaged density contours for $p_{0j} / p_{0x} = 1.633$
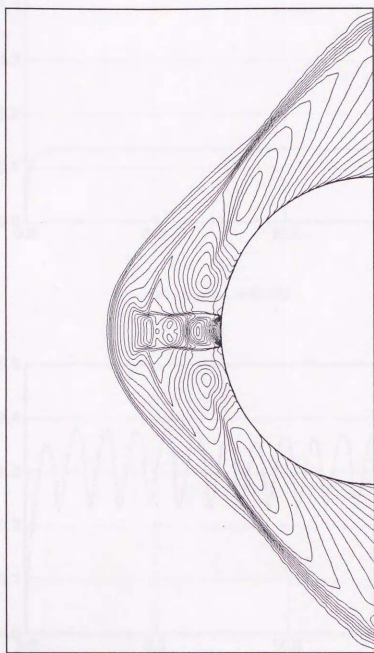
Figure 3.5   Time-averaged density contours for $p_{0j} / p_{0\infty} = 0.816$
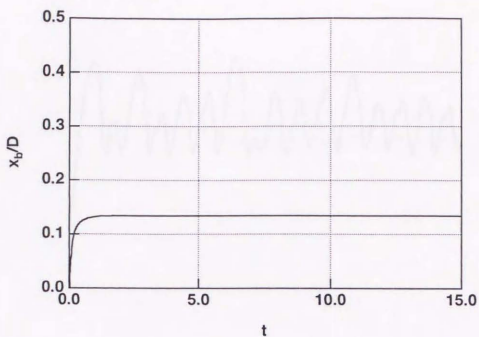
(a) $p_{0j}/p_{0\infty} = 0.491$
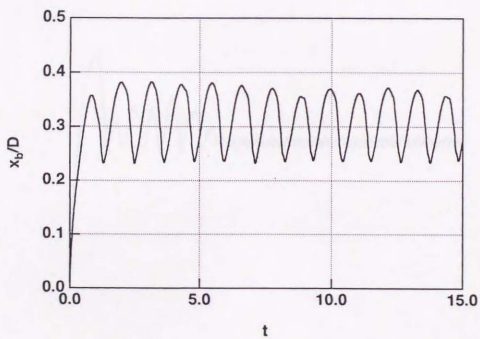
(b) $p_{0j}/p_{0\infty} = 0.816$

Figure 3.6   Time-variation of bow shock on the axis
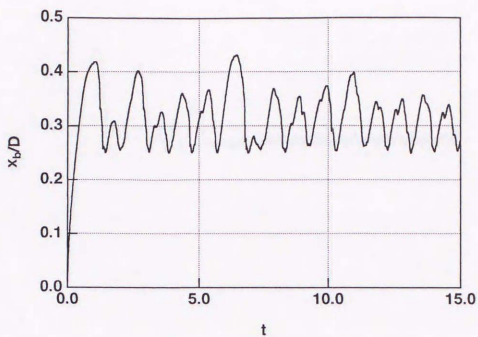
(c) $p_{0j}/p_{0\infty} = 0.968$
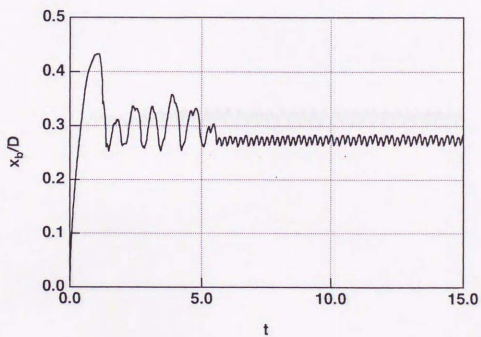
(d) $p_{0j}/p_{0\infty} = 1.005$

Figure 3.6   Continued
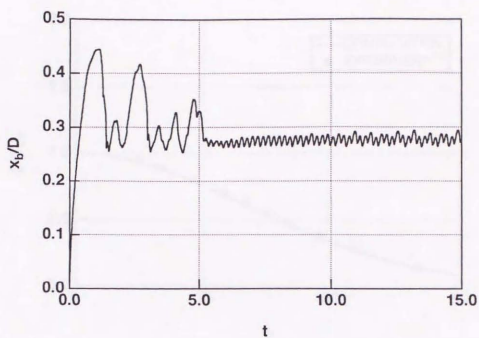
(e) $p_{0j}/p_{0\infty} = 1.036$
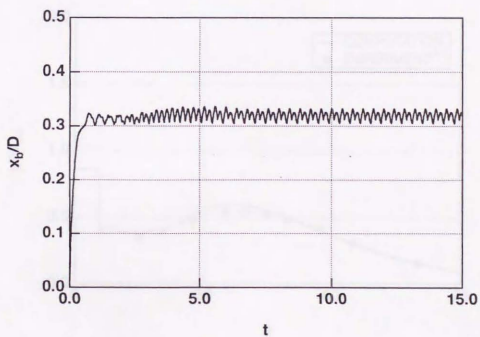
(f) $p_{0j}/p_{0\infty} = 1.633$

Figure 3.6   Continued
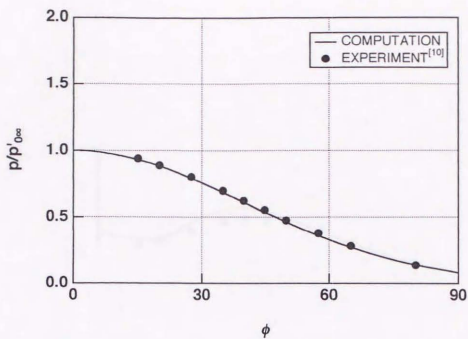
(a) $p_{0j}/p_{0\infty} = 0.491$
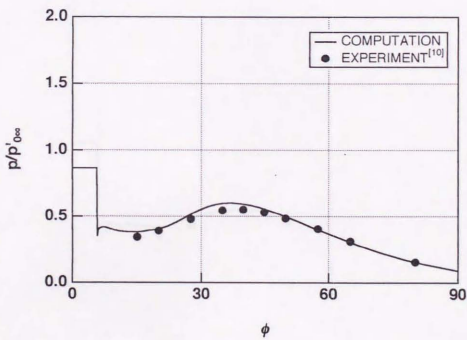
(b) $p_{0j}/p_{0\infty} = 0.816$

Figure 3.7   Time-averaged surface pressure distribution
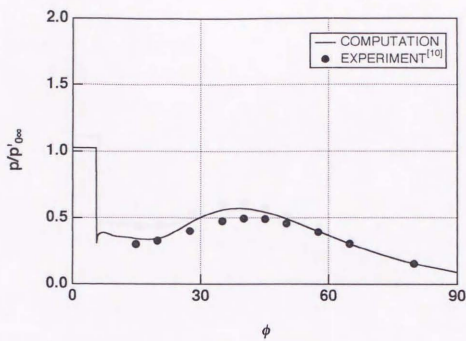
(c) $p_{0j}/p_{0\infty} = 0.968$
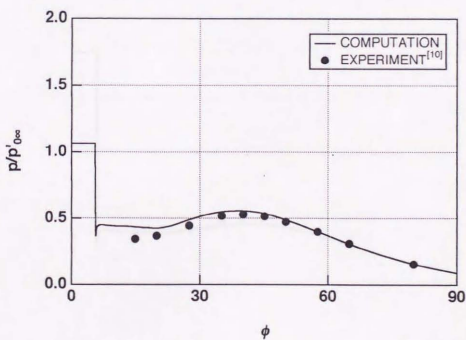
(d) $p_{0j}/p_{0\infty} = 1.005$

Figure 3.7   Continued
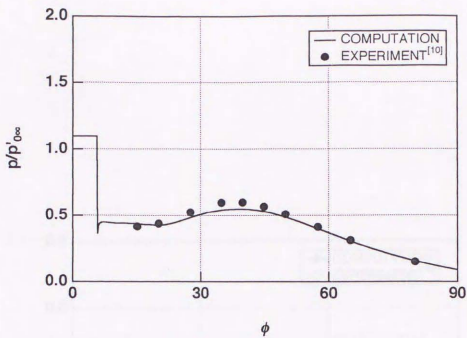
(e) $p_{0j}/p_{0\infty} = 1.036$
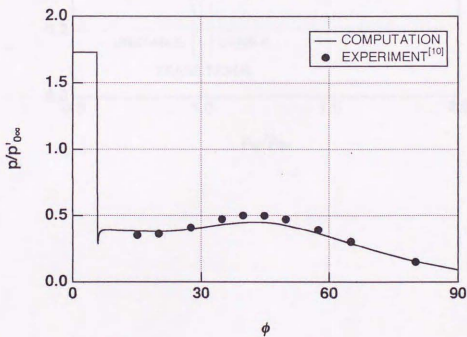
(f) $p_{0j}/p_{0\infty} = 1.633$

Figure 3.7   Continued
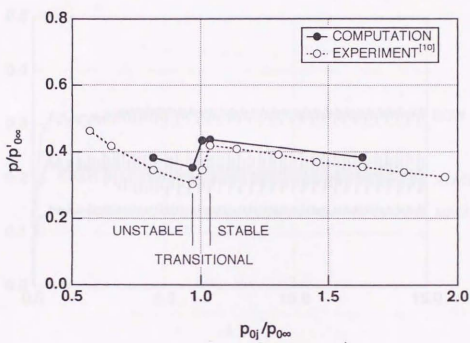
Figure 3.8   Pressure in the recirculating region versus total pressure ratio
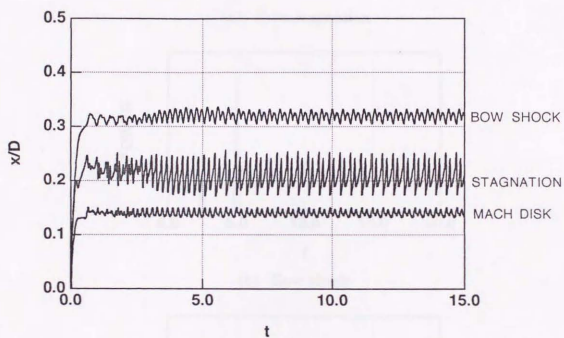
Figure 3.9   Time-variations of bow shock, Mach disk and stagnation
on the axis for $p_{0j}/p_{0\infty} = 1.633$
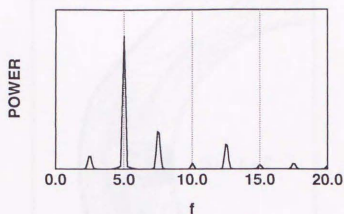
(a) Free stagnation
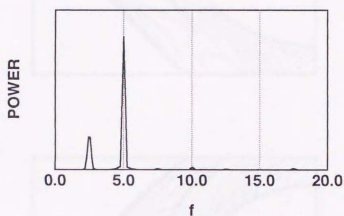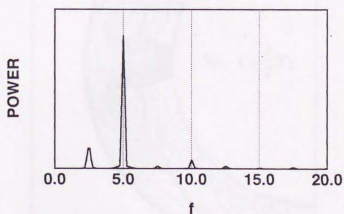
(b) Bow shock

(c) Mach disk

Figure 3.10   Power spectrums of time-varying solutions for $p_{0j}/p_{0\infty} = 1.633$

(a) $t = 0$

(b) $t = \frac{1}{7}T_1$
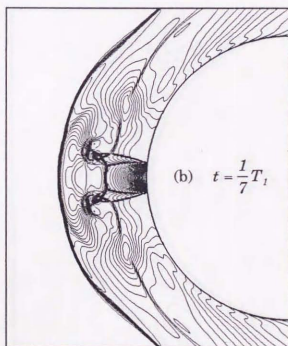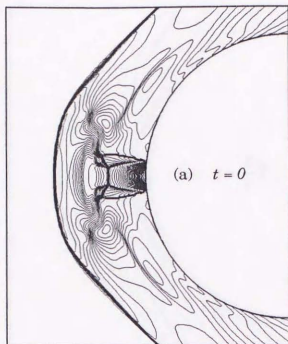
Figure 3.11   Time-variation of the flow field for $p_{0j} / p_{0\infty} = 1.633$

(c) $t = \frac{2}{7}T_1$

(d) $t = \frac{3}{7}T_1$

Figure 3.11 Continued

(e) $t = \dfrac{4}{7} T_1$

(f) $t = \dfrac{5}{7} T_1$

Figure 3.11   Continued

(g) $t = \frac{6}{7} T_1$

(h) $t = T_1$
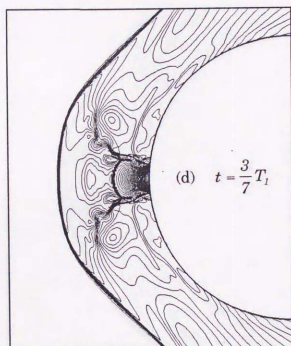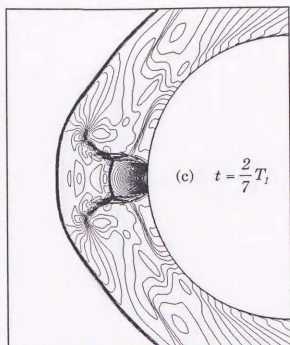
Figure 3.11   Continued
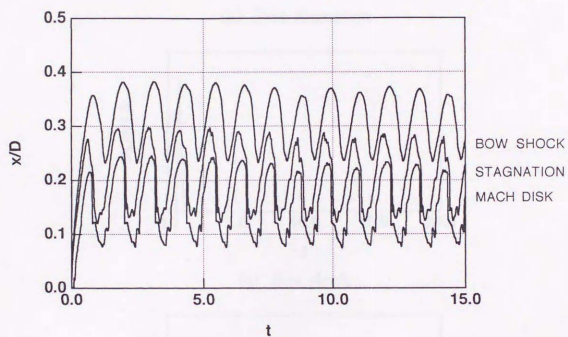
Figure 3.12   Time-variations of bow shock, Mach disk and stagnation
on the axis for $p_{0j}/p_{0\infty} = 0.816$
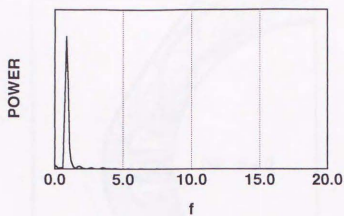
(a) Free stagnation
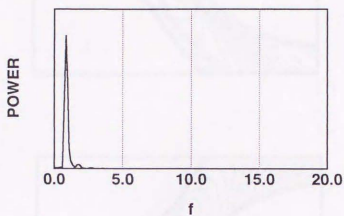
(b) Bow shock
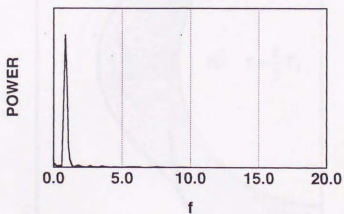
(c) Mach disk

Figure 3.13 Power spectrums of time-varying solutions for $p_{0j}/p_{0\infty} = 0.816$

(a) $t = 0$

(b) $t = \frac{1}{7}T_2$
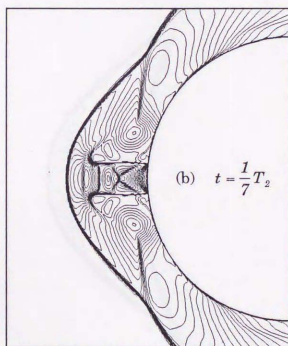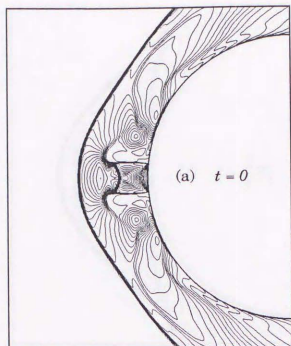
Figure 3.14   Time-variation of the flow field for $p_{0j} / p_{0\infty} = 0.816$

(c) $t = \dfrac{2}{7} T_2$

(d) $t = \dfrac{3}{7} T_2$

Figure 3.14   Continued

(e) $t = \dfrac{4}{7} T_2$

(f) $t = \dfrac{5}{7} T_2$

Figure 3.14   Continued

(g) $t = \dfrac{6}{7} T_2$

(h) $t = T_2$
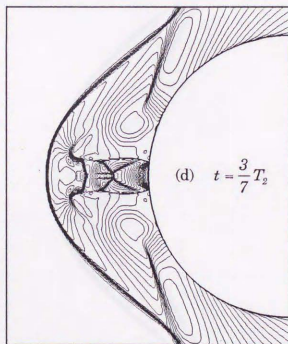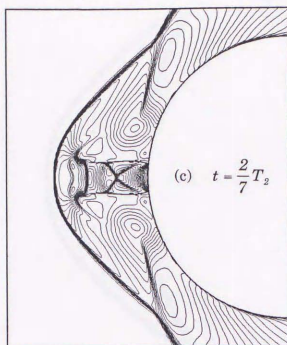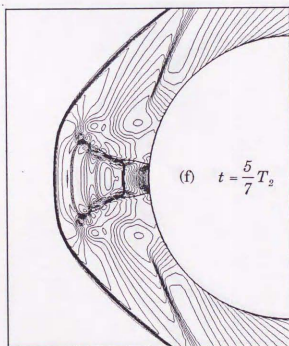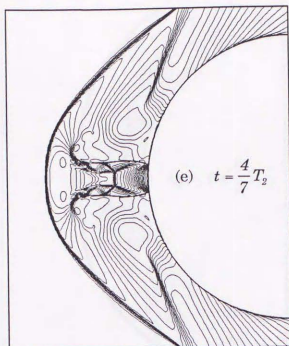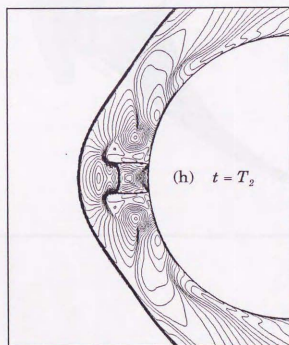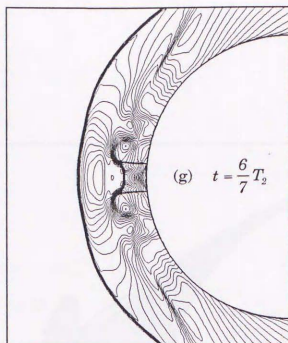
Figure 3.14   Continued
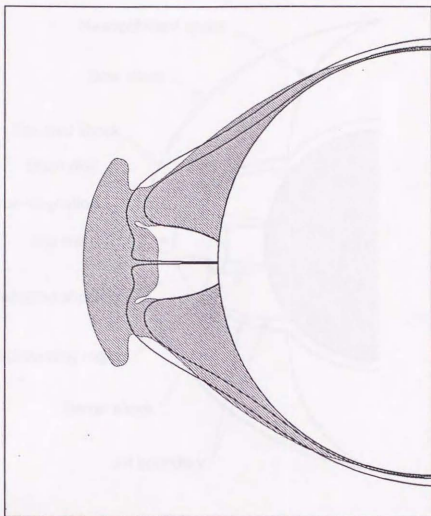
Figure 4.1   Subsonic region and jet stream lines of the time-averaged
flow field for $p_{0j} / p_{0\infty} = 1.633$
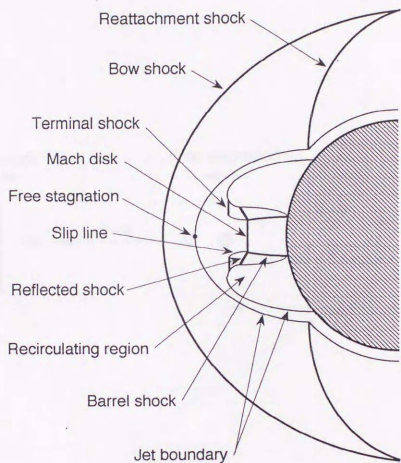
Figure 4.2 A flow model in the stable region
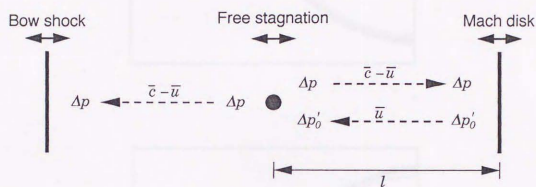
Figure 4.3   Propagation of small pressure disturbances along the axis
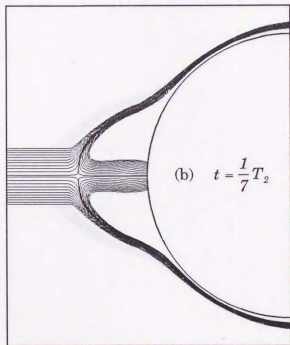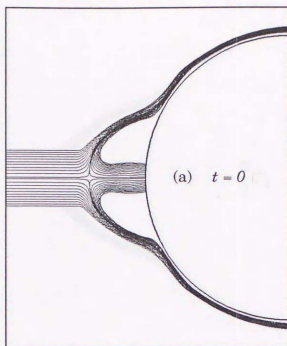
Figure 4.4   Time-variation of the instantaneous stream lines for

$p_{0j} / p_{0\infty} = 0.816$

(c) $t = \dfrac{2}{7} T_2$

(d) $t = \dfrac{3}{7} T_2$

Figure 4.4   Continued

(e) $t = \dfrac{4}{7}T_2$

(f) $t = \dfrac{5}{7}T_2$

Figure 4.4   Continued

(g) $t = \dfrac{6}{7} T_2$

(h) $t = T_2$
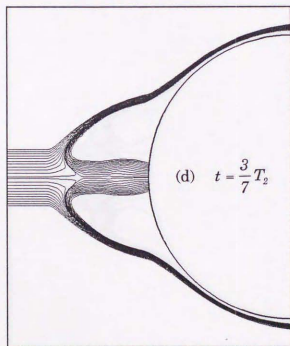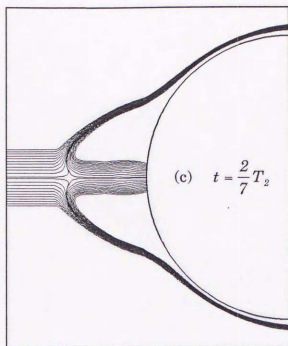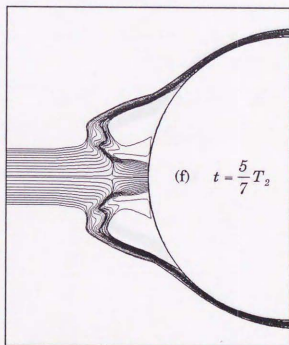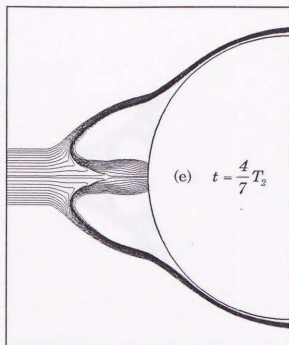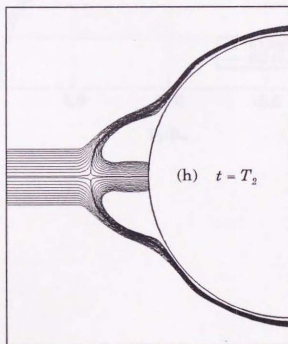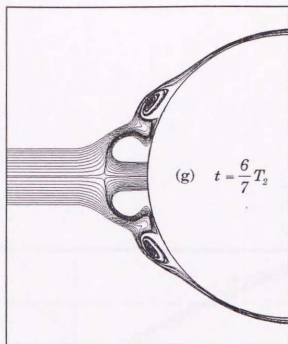
Figure 4.4   Continued
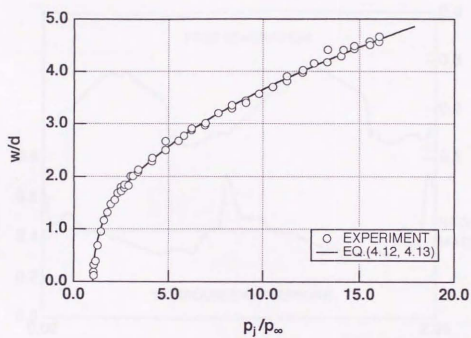
Figure 4.5   Length of the first jet cell versus jet static pressure ratio[52]
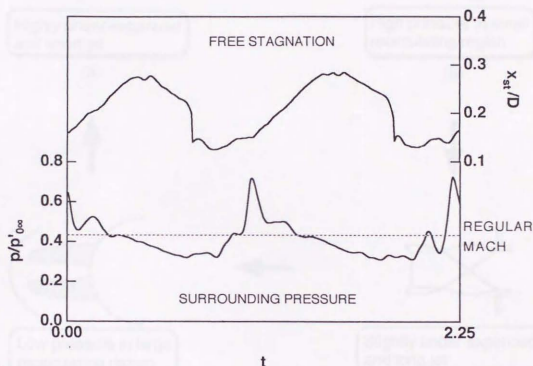
Figure 4.6   Time-variations of free stagnation and jet surrounding pressure
for $p_{0j}/p_{0\infty} = 0.816$
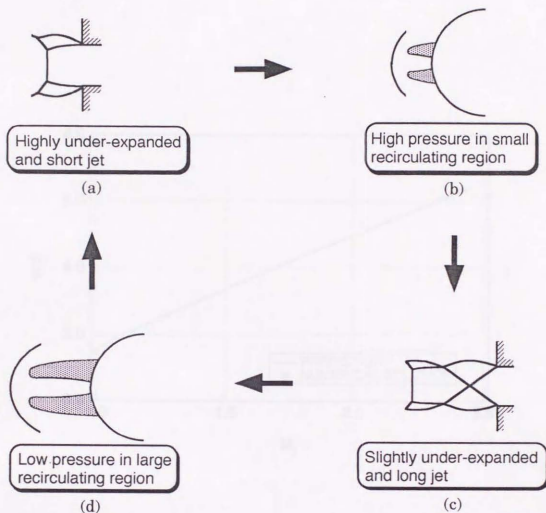
Figure 4.7 An oscillating flow model in the unstable region
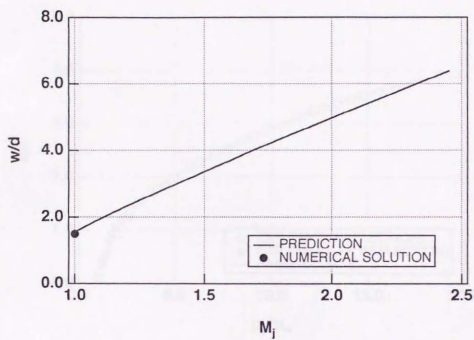
Figure 4.8   Amplitude of the large oscillation in the unstable region
versus jet exit Mach number
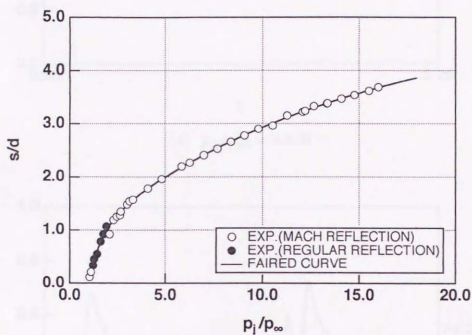
Figure 4.9   Distance from the jet exit to the intersecting shock on the axis
versus jet static pressure ratio[52]

(a) $p_{0j}/p_{0\infty} = 0.816$
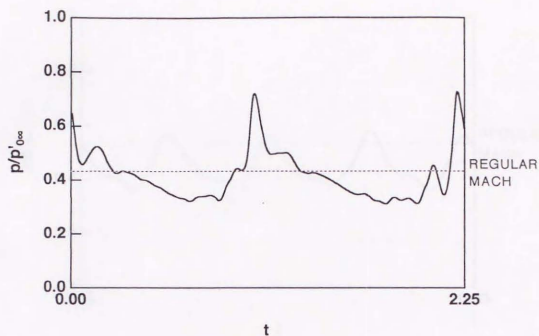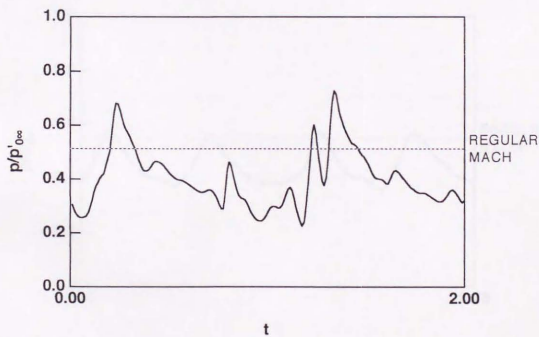
(b) $p_{0j}/p_{0\infty} = 0.968$

Figure 4.10   Time-variation of pressure in the recirculating region

(c) $p_{0j}/p_{0z} = 1.005$
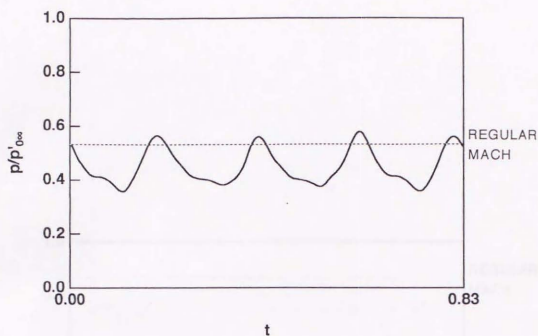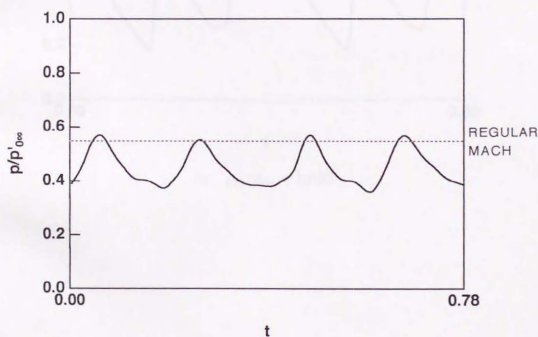
(d) $p_{0j}/p_{0z} = 1.036$

Figure 4.10 Continued
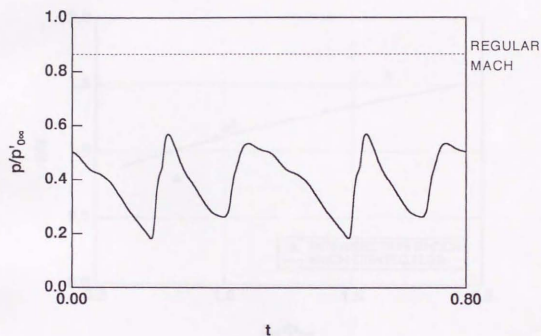
(e) $p_{0j}/p_{0\infty} = 1.633$

Figure 4.10 Continued
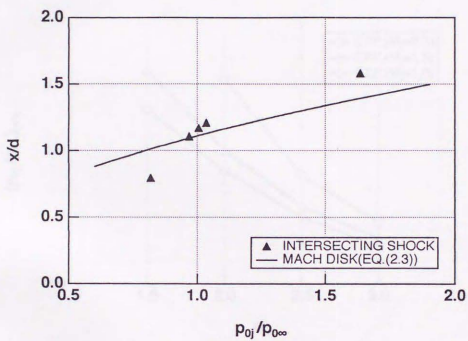
Figure 4.11   Distance to the intersecting shock and to the Mach disk
versus total pressure ratio
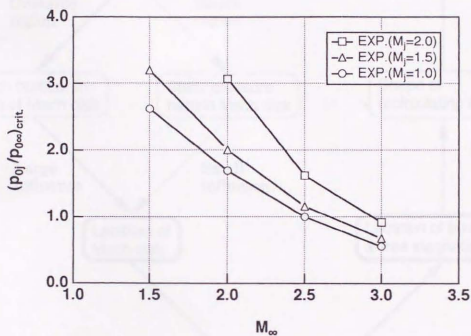
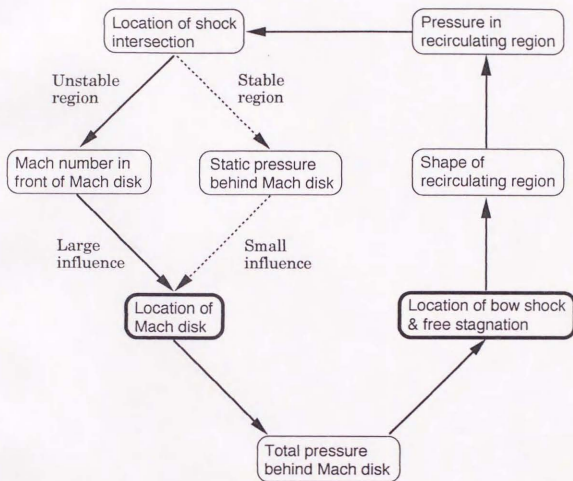Figure 4.12   Threshold of the transition versus free stream Mach number
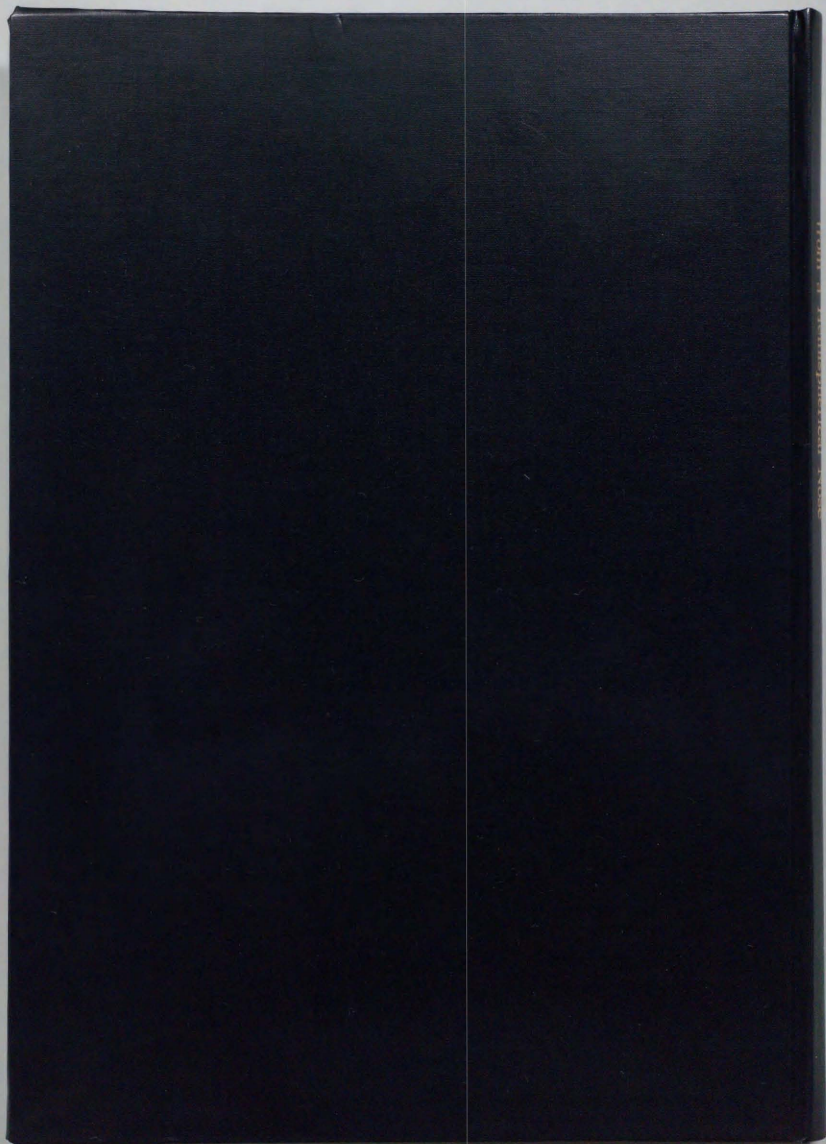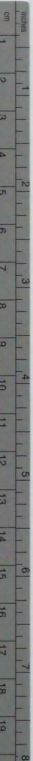and jet exit Mach number[10]

Figure 4.13   Feedback mechanism in the oscillatory opposing jet flow